UNIVERSITÀ DI PISA
DIPARTIMENTO DI SCIENZE DELLA TERRA

Pisa, August the 3rd, 2019

Dear Editor,

we submit a paper entitled

"**Strontium Isotope Stratigraphy of the Miocene sedimentary successions of the East Pisco Basin (Peru): new age constraints and paleoclimatic implications**"

by Giulia Bosio *et alii* for publication in *Journal of South American Earth Sciences* as a regular research article.

The marine deposits of the East Pisco Basin of southern Peru are of global interest because of their rich and exceptionally preserved fossil assemblage. Recent work has redefined and dated much of the local Miocene succession, comprising the lower Miocene Chilcatay and the upper Miocene Pisco formations. Crucially, however, a large gap remains between these two units, with the age of the lowest portion (P0 sequence) of the Pisco Formation remaining unknown. Here, we address this issue via Strontium Isotope ($^{87}Sr/^{86}Sr$) Stratigraphy dating carbonates (mollusks, barnacles, and nodules) and phosphates (shark teeth) from both formations. To avoid diagenetic bias, the suitability of shells was first assessed via optical and scanning electron microscopy, cathodoluminescence, and inductively coupled plasma-optical emission spectrometry. Likewise, only the best-preserved shark teeth were sampled for analysis. Our results confirm a Burdigalian age for the Chilcatay Formation and date P0 to the middle Miocene, which matches the relatively archaic aspect of its cetacean fossil assemblage. The depositional environment of P0 resembles the warm conditions associated with the Chilcatay Formation, rather than the cooler setting inferred for the remainder of the Pisco Formation. This pattern may reflect a middle or early late Miocene strengthening of the Humboldt Current.

We thought that this issue may be of interest for *Journal of South American Earth Sciences* and we decided thus to submit our work to Your attention. We would like to inform You that: 1) all the authors of this paper agree on its submission; 2) this article substantially relies on original data, it has not been published before, and is not concurrently being considered for publication elsewhere; 3) we have no competing interests; 4) this article does not violate any copyright or other personal proprietary right of any person or entity and it contains no abusive, defamatory, obscene or fraudulent statements, nor any other statements that are unlawful in any way.

We hope that our paper will interest You and will be suitable for publication in Your journal, and we look forward for receiving Your decision letter.

Sincerely Yours,
the Corresponding Author:

Giulia Bosio, PhD
Dipartimento di Scienze della Terra – Università di Pisa
via Santa Maria 53, 56126, Pisa (PI), Italy
E-mail address: giulia.bosio.giulia@gmail.com

Highlights for

Strontium Isotope Stratigraphy of the Miocene sedimentary successions of the East Pisco Basin (Peru): new age constraints and paleoclimatic implications

by Giulia Bosio et alii

- We applied Sr isotope dating to carbonates and phosphates from the East Pisco Basin

- $^{87}Sr/^{86}Sr$ values date the lower Pisco strata (P0 sequence) to the middle Miocene

- Paleontological data indicate a warm water paleoenvironment for P0

- Our results suggest a middle-late Miocene strengthening of the Humboldt Current

Strontium Isotope Stratigraphy of the Miocene sedimentary successions of the East Pisco Basin (Peru): new age constraints and paleoclimatic implications

Giulia Bosio[1,2]*, Elisa Malinverno[2], Alberto Collareta[1], Claudio Di Celma[3], Anna Gioncada[1], Mariano Parente[4], Fabrizio Berra[5], Felix G. Marx[6,7,8], Agostina Vertino[9], Mario Urbina[10], Giovanni Bianucci[1]

[1] Dipartimento di Scienze della Terra, Università di Pisa, 56126 Pisa, Italy

[2] Dipartimento di Scienze dell'Ambiente e della Terra, Università degli Studi di Milano-Bicocca, 20126 Milano, Italy

[3] Scuola di Scienze e Tecnologie, Università di Camerino, 62032 Camerino, Italy

[4] Dipartimento di Scienze della Terra, dell'Ambiente e delle Risorse, Università degli Studi di Napoli Federico II, 80126 Napoli, Italy

[5] Dipartimento di Scienze della Terra "Ardito Desio", Università di Milano, 20126 Milano, Italy

[6] Directorate of Earth and History of Life, Royal Belgian Institute of Natural Sciences, 1000 Brussels, Belgium

[7] School of Biological Sciences, Monash University, VIC 3800 Clayton, Victoria, Australia

[8] Palaeontology, Museums Victoria, VIC 3053 Melbourne, Victoria, Australia

[9] Department of Geology, Renard Centre of Marine Geology, Universiteit Gent, 9000 Ghent, Belgium

[10] Departamento de Paleontología de Vertebrados, Museo de Historia Natural, Universidad Nacional Mayor de San Marcos, Lima 1, Peru

* *Corresponding author. E-mail address: giulia.bosio.giulia@gmail.com*

Highlights

- We applied Sr isotope dating to carbonates and phosphates from the East Pisco Basin
- $^{87}Sr/^{86}Sr$ values date the lower Pisco strata (P0 sequence) to the middle Miocene
- Paleontological data indicate a warm water paleoenvironment for P0
- Our results suggest a middle-late Miocene strengthening of the Humboldt Current

Abstract

The marine deposits of the East Pisco Basin (Peru) are of global interest because of their rich and exceptionally preserved fossil assemblage. Recent work has redefined and dated much of the local Miocene succession, comprising the lower Miocene Chilcatay and the upper Miocene Pisco formations. Crucially, however, a large gap remains between these two units, with the age of the lowest portion (P0 sequence) of the Pisco Formation remaining unknown. Here, we address this issue via Strontium Isotope ($^{87}Sr/^{86}Sr$) Stratigraphy dating carbonates (mollusks, barnacles, and nodules) and phosphates (shark teeth) from both formations. To avoid diagenetic bias, the suitability of shells was first assessed via optical and scanning electron microscopy, cathodoluminescence, and inductively coupled plasma-optical emission spectrometry. Likewise, only the best-preserved shark teeth were sampled for analysis. Our results confirm a Burdigalian age for the Chilcatay Formation and date P0 to the middle Miocene, which matches the relatively archaic aspect of its cetacean fossil assemblage. The depositional environment of P0 resembles the warm conditions associated with the Chilcatay Formation, rather than the cooler setting inferred for the remainder of the Pisco Formation. This pattern may reflect a middle or early late Miocene strengthening of the Humboldt Current.

Keywords

$^{87}Sr/^{86}Sr$ stratigraphy, diagenesis evaluation, Miocene, mollusks, shark teeth, Cetacea

1. Introduction

The $^{87}Sr/^{86}Sr$ ratio of Sr (strontium) isotopes dissolved in the global ocean has varied through the geological time (McArthur, 1994; McArthur et al., 2012). At the same time, the world's seas are homogeneous with respect to $^{87}Sr/^{86}Sr$ ratio, and this is assumed for any

55 geologic time (McArthur et al., 2012). Therefore, Sr isotope composition can be used for
56 dating marine minerals and correlating marine sedimentary successions worldwide (Faure
57 and Mensing, 2005). Application of Strontium Isotope Stratigraphy (hereinafter: SIS)
58 requires measurement of the Sr isotope ratio of minerals that precipitated from seawater and
59 have not undergone diagenetic alteration of their original $^{87}Sr/^{86}Sr$ value (McArthur et al.,
60 2012). Some intervals of geological time, such as the Miocene, are particularly favorable for
61 implementation of SIS because they display high rates of change of the $^{87}Sr/^{86}Sr$ value and a
62 narrow error band on the empirically defined reference curve (McArthur et al., 2012), which
63 allow for high-resolution age estimates.
64 The Miocene Chilcatay and Pisco formations exposed in the East Pisco Basin of southern
65 Peru are renowned for their exceptional fossil assemblage, comprising cetaceans, seals,
66 sharks, rays, crocodiles, turtles, seabirds, and bony fishes (e.g., Bianucci et al., 2015, 2016 a,
67 b, c, 2018a, b; Collareta et al., 2017; Lambert et al., 2014, 2015, 2017 a, b, 2018; Landini et
68 al., 2017 a, b, 2019; Marx et al., 2017a, b; Gioncada et al., 2018b) as well as marine
69 invertebrates (e.g., DeVries and Frassinetti, 2003; DeVries et al., 2006; DeVries, 2016;
70 Coletti et al., 2018, in review; Collareta et al., 2019). To put this assemblage into context,
71 reliable age estimates are crucial. Recent work established a chronostratigraphic framework
72 based on ^{39}Ar–^{40}Ar dating, tephrostratigraphy and biostratigraphy, which dates the Chilcatay
73 Formation to the early Miocene and the upper sequences of the Pisco Formation to the late
74 Miocene, respectively (Di Celma et al., 2017, 2018a, b; Gariboldi et al., 2017; Bosio et al.,
75 2019, in press). The seemingly large temporal gap between these two units is striking, but is
76 almost certainly an overestimate caused by a lack of datable ash layers and microfossils from
77 the lowermost portion of the Pisco Formation (the P0 sequence). Previous studies remarked
78 on the significantly archaic aspect of the cetacean fauna from this layer (Di Celma et al.
79 2017; Marx et al. 2017b), but were unable to draw definitive conclusions as to its age. The

peculiar faunal changes that characterize this unit (Di Celma et al., 2017) make the dating of these strata an issue of prime importance for the ongoing paleontological studies on the Miocene fossil content of the East Pisco Basin.

Here, we present the first attempt to date the lower Pisco beds by means of SIS. Mollusk (i.e., ostreids and pectinids) and barnacle shells, diagenetic cements, bulk sediment samples, and shark teeth were collected to apply this method to both carbonates and phosphates. Several samples from the age-constrained Ct1 sequence of the Chilcatay Formation were dated for checking the reliability of the Sr results in the study areas. The preservation state of the invertebrate remains was preliminary addressed via petrographic, morphological, chemical, and cathodoluminescence analyses in order to quantify the extent of diagenetic alteration and to assess whether the shells were structurally and chemically pristine. Sr isotope ratios were elaborated with the LOWESS Table 5 made for the GTS2012 timescale (McArthur et al., 2012) and SIS ages were obtained.

Furthermore, we investigate the faunal assemblages of both fossil invertebrates and vertebrates for reconstructing the paleoenvironment of the P0 sequence. The paleoenvironmental and stratigraphic significance of this unit is then addressed in the light of our age estimates.

2. Geological setting

Since the Mesozoic, the geodynamics of Peru have been defined by the convergence of the oceanic Nazca/Farallon Plate and the continental South American Plate, creating a composite transform-convergent margin with a series of elongated extensional/pull-apart basins (e.g., Kulm et al., 1982; Dunbar et al., 1990; León et al., 2008; Zúñiga-Rivero et al., 2010). Two trench-parallel structural highs further divide the Peruvian offshore into a series of outer (i.e., seaward) and inner sedimentary basins (Thornburg and Kulm, 1981) (Fig. 1A). The East

Pisco Basin falls into the latter category, and today is evident as a 180 km-long depression paralleling the coast of southern Peru between the towns of Pisco and Nazca. Its rise above sea level is due to the subduction of the nearby Nazca Ridge, a region of topographically high oceanic crust impinging on the Peru-Chile trench (Pilger, 1981; Hsu, 1992; Macharé and Ortlieb, 1992; Hampel, 2002). The basin infill comprises, in stratigraphic order, the Eocene Caballas and Paracas formations, the upper Eocene to lower Oligocene Otuma Formation, and the largely Miocene Chilcatay and Pisco formations (Dunbar et al., 1990; DeVries, 1998, 2017; DeVries et al., 2017; DeVries and Jud, 2018). These units are bounded by regionally extensive unconformities marking major breaks in the sedimentary record, commonly demarcated by pavements of igneous pebble-boulder clasts indicative of subaerial exposure; moreover, intraformational unconformities are also present (DeVries, 1998; Di Celma et al., 2017, 2018a, b). Therefore, this succession has been classified using both a lithostratigraphic (formations) and an allostratigraphic (allomembers) approach (North American Commission on Stratigraphic Nomenclature [NACSN], 2005). In the present paper, we maintain the lithostragraphic classification for the formations and identify within them a number of informal units, defined in the study area by unconformities, as sequences (the unconformities observed in the study area are actually sequence boundaries). This subdivision could be applied also basinward, whenever these unconformities may pass to correlative conformities.

During deposition of the Chilcatay and Pisco formations, the East Pisco Basin was a semi-enclosed, shallow-marine bay, structured along a latitudinal depth gradient, and sheltered seawards by a longshore chain of crystalline basement islands (Fig. 1B) (Marocco and Muizon, 1988; DeVries and Jud, 2018; Bianucci et al., 2018b). The Chilcatay Formation is composed of two distinct sequences, namely, Ct1 and Ct2; the former includes three facies associations, recording deposition in shoreface, offshore, and subaqueous delta, whereas the latter includes two facies associations, recording deposition in shoreface and offshore settings

(Di Celma et al., 2018b, 2019). The chronostratigraphic framework of these outcrops is well constrained by integration of micropaleontological data and isotope geochronology. Diatom biostratigraphy suggests deposition of the Chilcatay sediments exposed at Ullujaya between 19 and 17 Ma (Burdigalian), whereas the $^{39}Ar–^{40}Ar$ radiometric age of an ash layer from the uppermost portion of the Ct2 sequence indicates deposition at 18.02 ± 0.07 Ma (Di Celma et al., 2018b; Bosio et al., in press). The Pisco Formation is composed of three fining-upward sequences, designated P0, P1, and P2 from oldest to youngest, which are divided by three unconformities, named PE0.0, PE0.1, PE0.2, respectively, and progressively onlap a composite basal unconformity from southwest to northeast. Each unit, representing a transgressive cycle, recorded deposition in shoreface (sandstones) and in offshore (siltstones/diatomaceous siltstones). The time of deposition of the P1 and P2 sequences is constrained, thanks to diatom biostratigraphy and $^{39}Ar–^{40}Ar$ ages of tephra, between 9.5 Ma and 8.6 Ma, and between 8.4 and 6.7 Ma, respectively (Gariboldi et al., 2017; Bosio et al., in press). Due to the lack of tephra layers and microfossils, the depositional age of the lower unit, P0, is to date very poorly constrained between 18.02 ± 0.07 Ma and 9.46 ± 0.05 Ma (Di Celma et al., 2017; Bosio et al., in press). Note, however, that DeVries and Jud (2018) previously proposed an early–middle Miocene age for the lower portion of the Pisco Formation (including P0), based on a series of diatom samples analyzed by H. Schrader in the 1980s.

3. Stratigraphy and fossil assemblage of the Ct1 and P0 sequences

At Ullujaya and Roca Negra, two localities along the western side of the Ica River (Fig. 2A), the lower sequence (Ct1) of the Chilcatay Formation consists of massive sandstones and conglomerates with boulder-sized clasts at the bottom (*Ct1c* facies association), followed by medium- to fine-grained sandstones alternating with conglomerate beds (*Ct1a*), and

clinobedded coarse-grained calcirudites at the top (*Ct1b*) (Di Celma et al., 2018b, 2019). These facies associations record deposition in the shoreface, offshore, and on a mixed siliciclastic-carbonate subaqueous delta, respectively (Di Celma et al., 2019), and suggest a semi-protected embayment associated with both a river mouth and the open ocean (Bianucci et al., 2018b).

The invertebrate fossil assemblage of Ct1 is concentrated into discrete layers, and comprises mollusks, barnacles, serpulids and echinids (Di Celma et al., 2018b). Bivalves are represented by ostreids, pectinids and venerids. Barnacles mainly belong to three taxa, with *Austromegabalanus carrioli* being the most abundant (Coletti et al., 2018; Collareta et al., 2019). The vertebrate fossil assemblage is dominated by toothed cetaceans (Odontoceti), including kentriodontids (*Kentriodon* sp.), squalodelphinids (*Notocetus vanbenedeni* and *Huaridelphis raimondii*), physeteroids (sperm whales), platanistid-like longirostrine homodont forms, eurhinodelphinids, and the eurhinodelphinid-like *Chilcacetus* (Bianucci et al., 2015, 2018b; Lambert et al., 2014, 2015; Di Celma et al., 2018b, 2019). In addition, there are sea turtles (large-sized indeterminate dermochelyids), bony fishes and elasmobranchs, with abundant juvenile teeth of the bronze shark *Carcharhinus brachyurus* and the extinct lamniform *Cosmopolitodus hastalis*. Overall, the fossil assemblage points to a coastal community dominated by warm-water mesopredators (Bianucci et al., 2018b).

The P0 strata of the Pisco Formation reach their maximum thickness (about 40 m) at the locality of Cerro Submarino. This unit is mostly composed of fine- to very coarse-grained, cross-stratified, fossil-rich sandstones, suggesting a very nearshore environment (Di Celma et al., 2017).

The fossil invertebrate assemblage is dominated by mollusks, with barnacles being less common. Bivalves primarily include *Chionopsis* spp. and *Dosinia ponderosa*, but *Miltha* cf. *vidali* and ostreids are also present. Gastropods mainly belong to the family

Architectonicidae, in addition to cypraeids and one specimen of *Ficus distans* (Di Celma et al., 2017). Finally, the assemblage includes the only known occurrence of a rhizangiid coral in the East Pisco Basin, reported in this paper for the first time.

Vertebrates are abundant, but less studied than those from the underlying Chilcatay strata (Di Celma et al., 2017; Marx et al., 2017b; Bianucci et al., 2019). Baleen whales (Cetacea: Mysticeti) dominate the assemblage and are represented by i) a large-sized stem balaenopteroid, *Pelocetus* sp.; ii) the archaic cetotheriid *Tiucetus rosae*, previously described from the southeastern locality of Santa Rosa (Marx et al., 2017b), but also present at other sites with better-constrained stratigraphy and P0 exposures along the western side of the lower Ica valley; and iii) a third form, previously identified as a cetotheriid (Di Celma et al., 2017), but here more conservatively reinterpreted as an indeterminate plicogulan. Toothed whales include at least one physeteroid and two kentriodontid-like delphinoids. In addition, there are fragmentary fossils of chelonioid turtles and longirostrine crocodilians, and a single bird specimen representing an indeterminate pelagornithid. Shark and ray teeth are relatively common and include, among others, *Anoxypristis* sp., *Carcharhinus* spp., *Carcharocles megalodon*, *Cosmopolitodus hastalis*, *Hemipristis serra*, *Isurus oxyrinchus* and myliobatids (eagle rays).

4. Material and Methods

4.1. Study area and sample collection

The study area is settled in the Ica desert, at the localities of Roca Negra and Ullujaya, where the Chilcatay Formation crops out (Di Celma et al., 2018b, 2019; Bianucci et al., 2018b), and Cerro Submarino, where P0 displays its maximum thickness (Fig. 2A).

Samples collected for applying the SIS were carbonates (invertebrate shells, cements) and phosphates (shark teeth). For the Sr isotope analyses, shark tooth fluorapatite and low-Mg

calcite shells were preferred, as low-Mg calcite is more stable, more resistant to diagenesis and less soluble than other carbonates (Brand, 1991; Steuber, 2003). Mollusks (i.e., ostreids and pectinids) and barnacles, shark teeth, and bulk and cement samples were collected along the measured section of the well-dated Chilcatay Formation at Roca Negra (14°39'04"S; 75°38'54"W) and Ullujaya (14°34'59"S; 75°38'27"W), as well as from the undated P0 deposits at Cerro Submarino (14°34'38"S; 75°39'51"W) (Fig. 2A). Different horizons were selected at each locality (Fig. 2B, C) and, for each level, several carbonate shells were sampled, usually from different organisms (e.g., oysters, pectinids, and barnacles). Some bulk and cement samples were also analyzed for better understanding the diagenetic path and its effects on $^{87}Sr/^{86}Sr$ values.

4.2. Optical microscopy (OM), scanning electron microscopy (SEM), and cathodoluminescence

Diagenetic processes or weathering could modify the pristine $^{87}Sr/^{86}Sr$ ratio of carbonate and phosphate marine minerals. As diagenetic or weathering modifications can affect the analytical results, providing wrong ages of mineral formation (Scasso et al. 2001; Brand et al. 2012; Ullmann and Korte, 2015), their identification is critical for evaluating the reliability of the $^{87}Sr/^{86}Sr$ ratio, which is suitable for SIS only when post-depositional alterations can be excluded. With the aim of evaluating the impacts of diagenesis and wethering on shells, mollusk and barnacle samples from both the Chilcatay and Pisco formations have been prepared for realizing thin sections. Petrographic analyses of polished thin sections were carried out through Leica and Olympus optical microscopes. A SEM-EDS Tescan VEGA TS Univac 5136XM was used at the Department of Earth and Environmental Sciences of the Università degli Studi di Milano-Bicocca for petrographic and morphological observations, as well as for checking evidence of dissolution in the structure of the selected shells.

Cathodoluminescence was performed using a CITL Optical Cathodoluminoscope at the Department of Earth Science "Ardito Desio" of the Università degli Studi di Milano, operated at about 14kV accelerating voltage and 0.5 mA gun current intensity. Cathodoluminescence observations permitted the identification of different carbonate generations, as well as of recrystallized portions of the shells (Barbin, 2013; Ullman and Korte, 2015).

Pristine shells were chosen for the age calculation, but some recrystallized materials were also selected for $^{87}Sr/^{86}Sr$ analyses, for understanding how diagenesis changed the Sr ratio (i.e., diagenesis path) (Steuber, 2003). Regarding shark teeth, samples were taken from the outer enameloid layer, avoiding dentine, which is generally more porous and susceptible to diagenetic alteration than enameloid (Becker et al., 2008; Enax et al., 2014).

After the preliminary analyses, fifteen samples were selected from the Ct1 sequence of the Chilcatay Formation, whereas eight samples were selected from the P0 sequence of the Pisco Formation (Table 1).

4.3. Compositional and strontium isotope analyses

After microscopic investigations, the selected pristine mollusk shells and well-preserved barnacle sheaths were carefully cleaned through an ultrasonic bath in distilled water. They were bored with a Dremel micro-drill to obtain shell powder from the diagenetically unaltered portion. After an ultrasonic bath in distilled water, the selected shark teeth were also scraped as powder of their unaltered, non-porous enameloid was collected with the micro-drill. About 10-50 mg of each sample were collected for inductively coupled plasma-optical emission spectroscopy (ICP-OES) and $^{87}Sr/^{86}Sr$ analyses, taking care to avoid contaminations.

ICP-OES and $^{87}Sr/^{86}Sr$ analyses were made at the Institute für Geologie, Mineralogie und Geophysik of the Ruhr-Universität of Bochum. ICP-OES analyses were made with a Thermo

Fisher Scientific iCAP 6500 DUO spectrometer for analyzing the concentrations of Sr, Ca (calcium), Mg (magnesium), Fe (iron), and Mn (manganese).

$^{87}Sr/^{86}Sr$ ratios were determined with a TIMS Finnigan MAT 262 solid source mass spectrometer with seven collectors, using a dynamic (peak-hopping) mode of measurement. The cut-off limit for a strontium run was an error of $\pm 2\sigma \leqslant 5 \times 10^{-6}$ for the $^{87}Sr/^{86}Sr$ ratio, with 100–200 ratios per run (typical duration: 110 ratios, lasting 2 h 15 min, plus the filament heating time). Two standards – NIST NBS 987 and USGS EN-1 – were used to calibrate the analysis. NIST NBS 987 was loaded directly onto the filament, to confirm the stability of the mass spectrometer. USGS EN-1, a powder derived from a modern *Tridacna* shell, underwent the same procedure as the other carbonate samples, to ensure the reproducibility of the entire analytical process. Thirty-four analyses of NIST NBS 987 resulted in a mean of 0.710240 ± 0.000023 (2σ), while 24 analyses of USGS EN-1 yielded 0.709153 ± 0.000019 (2σ). No Rb (rubidium) correction was applied, but Rb was nonetheless monitored during the entire run. When Rb levels exceeded the detection limit, the result was discarded and the measurement repeated.

The results of the $^{87}Sr/^{86}Sr$ analyses were corrected for the difference between the USGS EN-1 value used for the compilation of the reference curve (McArthur et al., 2012) and the USGS EN-1 Bochum mean value, and then converted into ages using the LOWESS Table 5, which is tied to the GTS2012 timescale (McArthur et al., 2012). The latter is still incomplete, therefore the results were rounded off to the nearest value. Following the method described by Frijia et al. (2015), when more than one sample was analyzed for a single layer, a mean $^{87}Sr/^{86}Sr$ value was calculated. The uncertainty for each stratigraphic level was calculated as 2 s.e. (i.e., standard error) from the standard deviation of the mean.

5. Results

280 *5.1. Diagenesis evaluation*

281 The Chilcatay and Pisco formations present notably divergent patterns of carbonate
282 preservation. In the Chilcatay Formation, fossil invertebrates are well-preserved and retain
283 their pristine calcitic shells. In contrast, in the Pisco Formation, calcitic shells are only
284 present in the P0 sequence, where examples of calcite recrystallization also occur, but not in
285 P1 and P2, where mollusks are only preserved as casts (Di Celma et al., 2017). For these
286 reasons, SIS could only be applied in the Ct1 and P0 sequences, once some caveats have been
287 taken into account.

288 At the macroscale, all of the bivalves selected for Sr analyses from both the units appear
289 well-preserved and composed of calcite. The oysters (Fig. 3A) are usually incided by
290 attachment traces by sponges and/or drill holes due to the predatory action of carnivorous
291 gastropods; in several cases, they preserve layers of unaltered nacre. The pectinids (Fig. 3B)
292 are also well-preserved, with small borings and some barnacle attachment traces
293 (*Anellusichnus*; Santos et al., 2005). By contrast, the barnacles (Fig. 3C) generally display
294 obvious signs of abrasion and lack their opercula; the best-preserved and less porous portion
295 of the shell is often constituted by the sheath, the thickened upper part of the inner wall.
296 Shark teeth selected for Sr analyses are moderately- to well-preserved; although two shark
297 teeth show a breakage surface in their root, they all have an intact thin layer of enameloid that
298 surrounds the pulp cavity and covers the surface of the tooth crown (Fig. 3D).

299 Microscopically, the best-preserved pectinids and ostreids are characterized by foliated
300 and prismatic calcite, respectively (Fig. 4A, C) (Cox et al., 1971). Both also have a low,
301 homogeneous luminescence, suggesting little or no diagenesis (Fig. 4B, D). Nevertheless,
302 some of the analyzed ostreids also have layers that are luminescent, documenting diagenetic
303 modifications. Microborings filled by luminescent calcite or terrigenous sediments, can be
304 observed. These infills must be avoided during sampling for Sr isotope analyses, because

305 they could have non-pristine Sr ratio (Fig. 4C, D). As reported also by Crippa et al. (2016),
306 fossil ostreids occasionally exhibit layers of sparry calcite replacing the pristine aragonitic
307 layers (i.e., myostracum) or filling the chambers once permeated by organic matter (Fig. 4E,
308 F). All those specimens that present similar features were discarded from the Sr analyses.
309 Several oysters from the Ct1 and P0 sequences that exhibit a generally low luminescence
310 have discrete luminescent layers that appear pristine and prismatic. For explaining this
311 feature, which has also been documented in modern oysters, Barbin (1991, 2013) argued that
312 luminescence may not be always a convincing indicator of diagenetic alteration for oysters,
313 because the absorption of Mn^{2+} by benthic organisms depends on various factors, such as
314 growth rate, ontogeny, bathymetry and salinity. To minimize the risk of diagenetic bias, we
315 conservatively discarded all the ostreid samples with diffuse microborings, sparry calcite, or
316 displaying high and/or heterogeneous luminescence. By contrast, the best-preserved
317 barnacles are characterized by low luminescence throughout the less porous portion of the
318 wall, but high luminescence charaterized the parietal tubes, which are normally filled with
319 secondary calcite (Fig. 4G, H). We carefully avoided to contact the parietal tubes during
320 sampling of the barnacle shells for the strontium analysis.
321 Secondary electron (SE) images confirmed the presence of alternating prismatic and
322 sparry calcite layers in some ostreid specimens (Fig. 5A, B) that were hence discarded. Other
323 specimens either retain a pristine prismatic layer (Fig. 5C) or show clear signs of alteration,
324 with the prismatic layer being unrecognisable, very irregular, or dissolved (Fig. 5D). Again,
325 specimens exhibiting obvious evidence of diagenesis were discarded.
326 ICP-OES analysis is useful for measuring the Fe, Mn, Mg, and Sr concentrations, which in
327 turn can be informative in terms of diagenetic imprint on carbonates. Usually, the Fe and Mn
328 contents of carbonates increase during the diagenetic processes; on the contrary, the Mg and
329 Sr contents generally decrease during diagenesis (Brand and Veizer, 1980; McArthur, 1994;

330 Steuber, 1999). In Figure 6A, the low Sr content of cement and bulk samples indicates a
331 decrease in Sr during diagenesis, as reported by Frijia and Parente (2008) for diagenetically
332 altered marine carbonates, coupled with a decrease of the $^{87}Sr/^{86}Sr$ value. The latter trend is
333 opposite to what is normal observed in diagenetically altered carbonates, when the interaction
334 of the diagenetic fluids with siliciclastic rocks generally results in more radiogenic Sr isotope
335 values (McArthur, 1994). The decrease of the Sr ratio in the diagenetically altered calcite of
336 the studied successions can be due to the pre-Miocene seawater-derived brine circulating
337 within the sedimentary sequence, as reported by Gioncada et al. (2018a). This decrease of the
338 Sr isotope ratio from pristine to diagenetic calcite confers older Sr ages to the diagenetically
339 altered samples. The abundance of Fe and Mn in the diagenetic samples (see Fig. 6B, C, D)
340 conforms to the expected pattern of increasing Fe and Mn concentration during diagenesis.
341 The above reconstruction of the diagenetic paths helps in assessing the preservation of each
342 sample. Indeed, samples displaying the same degree of morphological preservation but higher
343 concentrations of Sr and lower concentrations of Fe and Mn might be considered as retaining
344 the pristine Sr isotope ratio of seawater.
345
346 *5.2. Strontium Isotope Stratigraphy of the Ct1 sequence*
347 After discarding all those shells that may have been affected by post-depositional
348 modifications, fifteen samples from the Ct1 sequence of the Chilcatay Formation (Ullujaya
349 and Roca Negra) were selected for $^{87}Sr/^{86}Sr$ analysis (Table 2). From each locality, Sr isotope
350 analyses of different well-preserved shells yielded similar Sr isotope values. The internal
351 consistency of the Sr isotope ratios of different samples from the same stratigraphic level can
352 be regarded as a strong argument supporting the preservation of the original seawater
353 $^{87}Sr/^{86}Sr$ value (McArthur et al.,1994; Steuber, 2003).

354 At Roca Negra, we sampled three well-preserved oysters (PN-OST, PN-GIO1, PN-GIO2)
355 from the *Ct1c* facies association. The three specimens came from a single bed (PN Oyster
356 level; Fig. 2) close to the base of the formation, ten meters above an ash layer (PN-T2) dated
357 to 19.25 ± 0.05 Ma (Bosio et al., in press). Sr isotope analyses give similar $^{87}Sr/^{86}Sr$ results
358 (Table 2) and the mean value gives a preferred age of 18.50 with a range of uncertainty
359 spanning between 18.85 and 18.15 Ma (Table 3). This SIS age is in agreement with the older
360 age (i.e., 19.25 Ma) of the PN-T2 ash layer, sampled ten meters below.
361 At Ullujaya, we sampled 12 specimens from the *Ct1a* facies association, whose age is
362 constrained by a basal ash layer (UJA-T35) dated to 19.00 ± 0.28 Ma (Bosio et al., in press),
363 and by a second ash layer in the overlying *Ct2b* facies association (SOT-T3; Fig. 2) dated to
364 18.02 ± 0.07 Ma (Di Celma et al., 2018b).
365 Three samples – a barnacle sheath (UL-LIVa), composite sample of two pectinids (UL-
366 LIVb), and a further, single pectinid (UL-LIVc) – were chosen from a layer 9 m above the
367 base of the measured section (hereafter: abs), named "mollusk- and barnacle-rich horizon" by
368 Collareta et al. (2019) (Fig. 2). The mean value of the $^{87}Sr/^{86}Sr$ values gives again a preferred
369 age of 18.50 Ma and an uncertainty that ranges from 18.60 to 18.40 Ma for this horizon
370 (Table 3).
371 At 17 m abs, in occurrence of the key bed C (KbC of Di Celma et al., 2018b) (Fig. 2),
372 nacre layers of two well-preserved oysters were selected (UJA-LIVC1, UJA-LIVC3) together
373 with a barnacle sheath (UJA-LIVC4) (Table 1). In addition, a sample of the cemented bulk
374 sediment from the outer part of an oyster shell was also analyzed (UJA-LIVC2). Considering
375 only the ages from the pristine shells, we obtained similar $^{87}Sr/^{86}Sr$ values and Burdigalian
376 ages (see Table 2). The bulk sample UJA-LIVC2 shows a lower value of $^{87}Sr/^{86}Sr$ ratio and
377 gives older ages, suggesting an ageing effect caused by diagenesis, as discussed above. The
378 age range of the key bed C is thus comprised between 18.50 and 18.10 Ma, with a preferred

379 age of 18.30 Ma (Table 3). The SIS age of this bed is apparently younger than that of the bed
380 below (i.e., the mollusk- and barnacle-rich horizon), dated at ca. 18.50 Ma, although the two
381 obtained age ranges are still largely overlapping.

382 Three samples were selected for the UL-D4 bed, a carbonate-rich horizon located 25 m
383 abs (see Fig. 2): UL-D4a, from prismatic layers of an oyster; UL-D4b, from a barnacle
384 sheath; UL-D4c, the bulk sediment cemented within the same barnacle shell (Table 1). The
385 bulk sample, UL-D4c, exhibits a relatively low $^{87}Sr/^{86}Sr$ value and, consequently, a relatively
386 older age value, indicating that diagenesis had an ageing effect on the shells also in this bed.
387 Unfortunately, the $^{87}Sr/^{86}Sr$ values of the two supposedly pristine samples from this level are
388 very different. Since both these samples passed the diagenetic screening, we have no clue for
389 discarding one of them and retaining the other. Therefore, we decided to discard the samples
390 of the UL-D4 level from the age determination.

391 Finally, at 30 m abs, we took two samples (UJA-2a and UJA-2b) from different layers of a
392 single oyster shell, collected from key bed B of Di Celma et al. (2018b). The mean $^{87}Sr/^{86}Sr$
393 value provides a preferred age of 18.30 Ma for the key bed B, with a maximum age of 18.60
394 Ma and a minimum age of 18.00 Ma, in agreement with the levels dated below (Table 3).

395 The $^{87}Sr/^{86}Sr$ ages calculated for each bed confirm a Burdigalian age for the Ct1 sequence
396 of the Chilcatay Formation and are concordant with the $^{39}Ar–^{40}Ar$ ages of the ash layers and
397 biostratigraphic assessment of the studied Chilcatay outcrops. The time resolution of the SIS
398 method is not sufficient to discriminate the age of these closely spaced horizons. However,
399 the preferred ages of the sampled levels tend to be younger according to the stratigraphy
400 (except, as reported above, for the UL-D4 bed).

401

402 *5.3. Strontium Isotope Stratigraphy of the P0 sequence*

403 Carbonates from the P0 sequence are poorly preserved, resulting in just five samples from
404 a ~10 m-thick stratigraphic section located north of Cerro Submarino. Given the scarcity of
405 suitable carbonate samples, we also collected samples from well-preserved shark teeth
406 (phosphates). They show $^{87}Sr/^{86}Sr$ values that are consistent with those of the pristine
407 carbonate samples (see Fig. 6, Table 2). Taking also into account the limited thickness of the
408 P0 deposits exposed at Cerro Submarino, e we considered all the collected samples as
409 belonging to a single level and we calculated a unique $^{87}Sr/^{86}Sr$ age starting from five
410 different samples.
411 Three shark teeth were chosen from the lower portion of the P0 sequence, a few meters
412 above the PE0.0 unconformity, in the plain northward of Cerro Submarino (see Fig. 2). Of
413 the analyzed teeth, Tooth 1 is a lower anterolateral tooth of *Cosmopolitodus hastalis*, Tooth 2
414 is an upper tooth of the same species (Fig. 3D), and Tooth 3 is a lower tooth of *Isurus*
415 *oxyrinchus* (see Table 1). The three resulting $^{87}Sr/^{86}Sr$ values are slightly different from each
416 other, but there are no reasons to prefer one tooth over another and all these samples were
417 selected for the final age calculation.
418 A few meters above the PE0.0 unconformity, a calcite nodule from within a baleen whale
419 mandible (SUB-2, Table 1) was first selected following the hypothesis of precipitation during
420 early diagenesis, similarly to what hypothesized for the dolomite nodules found inside bone
421 cavities in the Pisco Formation (Gariboldi et al., 2015; Gioncada et al., 2016). However,
422 SUB-2 has a very low $^{87}Sr/^{86}Sr$ value similar to the late diagenetic cements, suggesting a late
423 diagenetic imprint of this nodule, and therefore it was discarded. Close to this sample, an
424 oyster was collected (SUB-5, Fig. 2), and the thin nacre layers were drilled, giving an
425 $^{87}Sr/^{86}Sr$ value similar to those of the shark teeth. Finally, a few meters above, three samples
426 were selected from level SUB-8bis (see Fig. 2): one from the presumably pristinely preserved
427 sheath of a barnacle (SUB-8bis1), one from the bulk sediment cemented inside the same

barnacle shell (SUB-8bis2), and the last one from a completely recrystallized shell of a bivalve (SUB-8bis3) (Table 1). The samples from the bulk and the recrystallized bivalve indicate that, as in the Ct1 sequence, diagenesis resulted in a substantial reduction of the $^{87}Sr/^{86}Sr$ value and a consequent increase of the calculated ages. In turn, the pristine calcite of the barnacle sheath shows an $^{87}Sr/^{86}Sr$ value similar to the other pristine samples and was considered for the final age calculation.

Discarding samples affected by diagenesis, a mean $^{87}Sr/^{86}Sr$ value can be calculated starting from 5 samples collected from the lower part of the P0 sequence. Together, the three shark teeth, SUB-5, and SUB8bis1 result in a mean age of 13.45 Ma, with an uncertainty time range spanning between 14.80 and 12.45 Ma. Consequently, by means of SIS, the P0 sequence can be placed in the Langhian–Serravallian (Table 3). The age of the P0 sequence is now resolved, but poorly constrained because of the scarcity of well-preserved specimens (allowing for just a few dated samples) and the intrinsic limits of the SIS method.

6. Discussion

6.1. SIS age of the P0 strata

Strontium data confirm a Burdigalian age for the Ct1 sequence of the Chilcatay Formation, in line with the $^{39}Ar–^{40}Ar$ dating on tephra and with the biostratigraphic results given by diatoms and silicoflagellates from the localities of Roca Negra and Ullujaya (Belia and Nick, 2016; Di Celma et al., 2018b; Bosio et al. in press). In addition, they are consistent in themselves, with stratigraphically lower beds yielding older or at least matching ages, although this observation is limited by the broadly overlapping error ranges for each layer. Overall, the consistency of the strontium dates from the Ct1 sequence confirms the suitability of the method for dating sediments in the East Pisco Basin.

Our results also provide the first direct evidence for the age of the P0 sequence of the Pisco Formation in the study area, placing this unit in the middle Miocene (Langhian–Serravallian). This estimate is again consistent with the broad age constraints (ca. 9.5–18.0 Ma) imposed by radiometric dating and biostratigraphy (Di Celma et al., 2018b; Bosio et al., in press).

Current knowledge about both invertebrate and vertebrate assemblages of the P0 sequence is poorly informative in terms of chronostratigraphy; that said, a middle Miocene age matches the general aspect of the P0 oryctocoenosis. Indeed, mollusks suggest similarities with the lower–middle Miocene Navidad Formation of central Chile (DeVries and Frassinetti, 2003). Likewise, the baleen whale assemblage appears remarkably more archaic than that of the overlying P1 and P2 sequences (Di Celma et al., 2017; Marx et al., 2017b), with the presence of *Pelocetus* sp. (Bianucci et al., 2019) matching other early–middle Miocene occurrences of this genus from Japan (Kimura et al., 2007) and eastern North America (Kellogg, 1965). Also notable is the abrupt increase in baleen whale abundance relative to the underlying Chilcatay Formation (Bianucci et al., 2018b), which appears to reflect a global early–middle Miocene pattern (Marx et al., 2019). Sharks and rays are of limited utility, as all the taxa recognized so far exhibit a stratigraphic range which spans for most of the Miocene at least. As a consequence, all the elasmobranch taxa recognized from the P0 sequence but *Carcharocles megalodon* and *Hemipristis serra,* are known from both the lower Miocene Chilcatay strata exposed in the Ullujaya-Zamaca areas (Bianucci et al., 2018b; Di Celma et al, 2018, 2019; Landini et al., 2019) and the upper Miocene Pisco strata (P1 and P2 sequences) exposed at Cerro Colorado (Di Celma et al., 2017; Landini et al., 2017a, b). *Carcharocles megalodon*, whose fossil record starts with the Burdigalian (Carrillo-Briceño et al., 2019, but see also Perez et al., 2019, at this regard), is well-known from the P1 and P2 beds but absent from the Chilcatay Formation, where the genus *Carcharocles* is represented by the more archaic

477 species *C. chubutensis*. Conversely, *Hemipristis serra* is present in the Burdigalian deposits
478 of the Chilcatay Formation, whereas it is absent from the younger P1 and P2 sequences,
479 although it is known from outside the East Pisco Basin in deposits as young as the early
480 Pleistocene (Ebersole et al., 2017).
481
482 *6.2. Paleoclimatic implications*
483 Previous investigations on the invertebrate assemblages from the P0 and P1 sequences
484 revealed a marked faunal change coincident with the PE0.1 unconformity (Di Celma et al.,
485 2017). Specifically, species such as *Ficus distans* and *Miltha* cf. *vidali*, which also occur in
486 the Chilcatay Formation, associate P0 with the Navidad Formation of Chile, rather than the
487 Panamic fauna (DeVries, 2002, 2007; DeVries and Frassinetti, 2003). According to Nielsen
488 and Glodny (2009), an interpretation of the mollusk assemblage from the Navidad Formation
489 in the light of the ecological preference of extant genera suggests water temperatures of at
490 least 20°C for the Navidad area (34°S) during the early-middle Miocene. Indeed, the presence
491 in the P0 sequence of warm-water or tropical taxa such as Architectonicidae and Cypraeidae
492 (see Fig. 7A–C, H–J), as well as the occurrence of *Ficus*, indicates a warm-water, tropical
493 paleoenvironment for this unit. This is also supported by the finding of the only coral colony
494 ever collected from the East Pisco Basin, belonging to the family Rhizangiidae (Fig. 7F, G).
495 Rhizangiid scleractinians are the most common corals in shallow-water tropical and warm
496 temperate environments of the eastern Pacific (Cairns et al., 2005); in particular, the P0
497 specimens appear as morphologically close to the Miocene to Holocene genus *Culicia*, which
498 currently lives in the tropical waters of the Indo-Pacific region. On the whole, these
499 observations support the paleoclimatic reconstruction proposed by DeVries and Frassinetti
500 (2003), who hypothesized warm-water conditions for the southern Peruvian coast during the

early and middle Miocene, in contrast with the cooler conditions during the late Miocene and early Pliocene.

Our data on the composition of the vertebrate oryctocoenosis from P0 also indicate tropical to subtropical thermal affinities for the paleoenvironment testified by the sandy strata that comprise the P0 sequence. In particular, among the recognized taxa, the knifetooth sawfish *Anoxypristis* is currently known as a nectobenthic organism that inhabits coastal and estuarine warm-water environments (e.g., D'Anastasi, 2013). Similarly, the extinct snaggletooth shark *Hemipristis serra* (Fig. 7D, E) is one of the most common chondrichthyan taxa in low-latitude neritic deposits of the Neogene, and its closest extant relative (*Hemipristis elongata*) is known as a tropical nearshore shark that inhabits coastal waters not deeper than about 30 m (e.g., Compagno, 1984). Interestingly, there are no late Miocene occurrences of *H. serra* from the East Pisco Basin, even though this species persisted till the early Pleistocene in many tropical/subtropical chondrichthyan assemblages worldwide, and has even been recorded from the late Miocene strata of the Miramar Formation of northern Peru (Apolín et al., 2004). A warm, tropical paleoenvironment sets P0 apart from the remainder of the Pisco Formation, which is thought to reflect a cooler setting marked by strong coastal upwelling (Dunbar et al. 1990; Di Celma et al. 2017). Overall, this pattern is suggestive of late Miocene cooling along the Peruvian coast (DeVries and Frassinetti, 2003), and therefore likely a strengthening of the Humboldt Current. This change might also explain the local disappearance of *H. serra*, whose range likely contracted northwards as colder conditions took hold along the coasts of southern Peru.

7. Conclusions

Along the western side of the Ica River (Peru), the age of deposition of the P0 sequence, the lowest stratigraphic unit of the Pisco Formation, was an uncertain and debated issue. In the

present study, Strontium Isotope Stratigraphy was applied on carbonates and phosphates of both the Chilcatay and Pisco formations for resolving the age of this paleontologically significant unit.

In order to obtain reliable ages, not offset by diagenetic effects, samples were screened by means of optical and scanning electron microscopy, cathodoluminescence, and ICP-OES analyses, and only the best-preserved specimens were selected for the subsequent Sr analyses.

In this work, we provide new Burdigalian ages (18.8–18.0 Ma) for the Ct1 sequence of the Chilcatay Formation and propose a Langhian–Serravallian age (14.8–12.4 Ma) for the P0 sequence of the Pisco Formation. This estimate is consistent with the relatively archaic aspect of the fossil assemblage from the lower Pisco strata, and provides a time constraint for a marked faunal change occurring across the PE0.1 unconformity. With respect to the Chilcatay Formation, the obtained Sr ages perfectly agree with previous ^{39}Ar–^{40}Ar ages on tephra layers and biostratigraphic results, confirming the feasibility of SIS in the studied deposits. This gives further reliability to the middle Miocene ages obtained by means of Sr isotope analyses for the P0 sequence.

Not least, both the invertebrate and vertebrate fossil assemblages indicate that the P0 sequence was deposited in a warm-water environment resembling that of the Chilcatay Formation, but contrasting with the cooler and more productive setting of the P1 and P2 sequences. We suggest that the marked cooling distinguishing P0 from the remainder of the Pisco Formation may reflect a middle–late Miocene strengthening of the Humboldt Current.

Acknowledgments

We thank T.J. DeVries for information and helpful discussions on the age and paleoenvironment of the Pisco Formation; W. Landini, O. Lambert and C. de Muizon for helpful discussions on the vertebrate fauna; D. Basso and G. Coletti for helpful discussions

551 on mollusk systematics and strontium dating; R. Varas-Malca and W. Aguirre for assistance
552 in the field; D. Buhl for running the ICP-OES and Sr isotope analyses at Bochum University;
553 and J. McArthur for sharing the LOWESS 5 Table.

554

555 **Funding**

556 This work was supported by grants from the Italian Ministero dell'Istruzione
557 dell'Università e della Ricerca (PRIN Project 2012YJSBMK) to G.Bi.; from the Università
558 degli Studi di Milano-Bicocca to E.M. (2017-ATE-0466); from the Università di Pisa to
559 G.Bi. (PRA_2017_0032); and an EU Marie Skłodowska-Curie Global Postdoctoral
560 fellowship (656010/ MYSTICETI) and an Australian Research Council DECRA fellowship
561 (DE190101052) to F.G.M.

562

563 **References**

564 Apolín, J., González, G., Martínez, J.M. (2004). Seláceos del Mioceno Superior de Quebrada
565 Pajaritos (Piura, Perú). Actas XII Congreso Peruano de Geología, Sociedad Geológica del
566 Perú, Perú, 401-404.

567 Barbin, V., Ramseyer, K., Debenay, J.P., Schein, E., Roux, M., Decrouez, D. (1991).
568 Cathodoluminescence of recent biogenic carbonates: an environmental and ontogenetic
569 fingerprint. Geological Magazine, 128, 19-26.

570 Barbin, V. (2013). Application of cathodoluminescence microscopy to recent and past
571 biological materials: a decade of progress. Mineralogy and Petrology, 107, 353-362.

572 Becker, A.M., Seidemann, D.E., Chamberlain, J.A. Jr., Buhl, D., Slattery, W. (2008).
573 Strontium isotopic signatures in the enameloid and dentine of upper Cretaceous shark
574 teeth from western Alabama: Paleoecologic and geochronologic implications.
575 Palaeogeography, Palaeoclimatology, Palaeoecology, 264, 188-194.

576 Belia, E.R., Nick, K.E. (2016). Early-Miocene calcareous nannofossil biostratigraphy from
577 low-latitude, Pisco Basin, Peru. Geological Society of America Abstracts with Programs,
578 48, 4.
579 Bianucci, G., Collareta, A., Bosio, G., Landini, W., Gariboldi, K., Gioncada, A., Lambert, O.,
580 Malinverno, E., de Muizon, C., Varas-Malca, R., Villa, I.M, Coletti, G., Urbina, M., Di
581 Celma, C. (2018b). Taphonomy and palaeoecology of the lower Miocene marine
582 vertebrate assemblage of Ullujaya (Chilcatay Formation, East Pisco Basin, southern Peru).
583 Palaeogeography, Palaeoclimatology, Palaeoecology, 511, 256-279.
584 Bianucci, G., Di Celma, C., Collareta, A., Landini, W., Post, K., Tinelli, C., de Muizon, C.,
585 Bosio, G., Gariboldi, K., Gioncada, A., Malinverno, E., Cantalamessa G., Altamirano-
586 Sierra, A, Salas-Gismondi, R., Urbina, M., Lambert, O. (2016a). Fossil marine vertebrates
587 of Cerro Los Quesos: Distribution of cetaceans, seals, crocodiles, seabirds, sharks, and
588 bony fish in a late Miocene locality of the Pisco Basin, Peru. Journal of Maps, 12, 1037-
589 1046.
590 Bianucci, G., Di Celma, C., Landini, W., Post, K., Tinelli, C., de Muizon, C., Gariboldi, K.,
591 Malinverno, E., Cantalamessa, G., Gioncada, A., Collareta, A., Salas-Gismondi, R., Varas-
592 Malca, R.M., Urbina, M., Lambert, O. (2016b). Distribution of fossil marine vertebrates in
593 Cerro Colorado, the type locality of the giant raptorial sperm whale Livyatan melvillei
594 (Miocene, Pisco Formation, Peru). Journal of Maps, 12, 543-557.
595 Bianucci, G., Urbina, M., Lambert, O. (2015). A new record of *Notocetus vanbenedeni*
596 (Squalodelphinidae, Odontoceti, Cetacea) from the early Miocene of Peru. Comptes
597 Rendus Palevol, 14, 5-13.
598 Bianucci, G., Bosio, G., Malinverno, E., de Muizon, C., Villa, I. M., Urbina, M., Lambert, O.
599 (2018a). A new large squalodelphinid (Cetacea, Odontoceti) from Peru sheds light on the
600 Early Miocene platanistoid disparity and ecology. Royal Society Open Science, 5, 172302.

601 Bianucci, G., Marx, F.G., Collareta, A., Di Stefano, A., Landini, W., Morigi, C., Varola, A.
602 (2019). Rise of the titans: baleen whales became giants earlier than thought. Biology
603 Letters, 15, 20190175.
604 Bosio, G., Gioncada, A., Malinverno, E., Di Celma, C., Villa, I. M., Cataldi, G., Gariboldi,
605 K., Collareta, A., Urbina, M., Bianucci, G. (2019). Chemical and petrographic
606 fingerprinting of volcanic ashes as a tool for high-resolution stratigraphy of the upper
607 Miocene Pisco Formation (Peru). Journal of the Geological Society, 176, 13-28.
608 Bosio, G., Malinverno, E., Villa, I.M., Di Celma, C., Gariboldi, K., Gioncada, A., Barberini,
609 B., Urbina, M., Bianucci, G. (in press). Tephrochronology and chronostratigraphy of the
610 Miocene Chilcatay and Pisco formations (East Pisco Basin, Peru). Newsletter on
611 Stratigraphy, DOI: 10.1127/nos/2019/0525.
612 Brand, U. (1991). Strontium Isotope Diagenesis of Biogenic Aragonite and Low-Mg Calcite.
613 Geochimica et Cosmochimica Acta, 55, 505-513.
614 Brand, U., Jiang, G., Azmy, K., Bishop, J., Montanez, I.P. (2012). Diagenetic evaluation of a
615 Pennsylvanian carbonate succession (Bird Spring Formation, Arrow Canyon, Nevada,
616 U.S.A.) — 1: Brachiopod and whole rock comparison. Chemical Geology, 308/309, 26-
617 39.
618 Brand, U., Veizer, J. (1980). Chemical Diagenesis of a Multicomponent Carbonate System -
619 1: Trace Elements. Journal of Sedimentary Research, 50, 1219-1236.
620 Cairns, S.D., Häussermann, V., Försterra, G. (2005) A review of the Scleractinia (Cnidaria:
621 Anthozoa) of Chile, with the description of two new species. Zootaxa, 1018, 15-46.
622 Carrillo-Briceño, J.D., Maxwell, E., Aguilera, O.A., Sánchez, R., Sánchez-Villagra, M.R.
623 (2015). Sawfishes and other elasmobranch assemblages from the Mio-Pliocene of the
624 South Caribbean (Urumaco Sequence, Northwestern Venezuela). PLOS ONE, 10, article
625 #e0139230.

626 Coletti, G., Bosio, G., Collareta, A., Buckeridge, J., Consani, S., El Kateb, A. (2018).
627 Palaeoenvironmental analysis of the Miocene barnacle facies: case studies from Europe
628 and South America. Geologica Carpathica, 69, 573-592.
629 Coletti, G., Collareta, A., Bosio, G., Buckeridge, J., Urbina M. (in review). *Perumegabalanus*
630 *calziai* gen. et sp. nov., a new intertidal megabalanine barnacle from the early Miocene of
631 Peru. Neues Jahrbuch für Geologie und Paläontologie-Abhandlungen, in review.
632 Collareta, A., Coletti, G., Bosio, G., Buckeridge, J., de Muizon, C., DeVries, T.J., Varas-
633 Malca, R., Altamirano-Sierra, A., Urbina-Schmitt, M., Bianucci, G. (2019). A new
634 barnacle (Cirripedia: Neobalanoformes) from the early Miocene of Peru: Palaeoecological
635 and palaeobiogeographical implications. Neues Jahrbuch für Geologie und Paläontologie-
636 Abhandlungen, 292, 321-338.
637 Collareta, A., Landini, W., Chalcatana, C., Valdivia, W., Altamirano-Sierra, A., Urbina-
638 Schimtt, M., Bianucci, G. (2017). A well preserved skeleton of the fossil shark
639 *Cosmopolitodus hastalis* from the late Miocene of Peru, featuring fish remains as
640 fossilized stomach contents. Rivista Italiana di Paleontologia e Stratigrafia, 123, 11-22.
641 Compagno, L.J.V. (1984). FAO Species Catalogue. Vol 4: Sharks of the world, Part 2 -
642 Carcharhiniformes. FAO Fisheries Synopsis No. 125, 4 (2), 251-633.
643 Cox, L.R., Newell, N.D., Boyd, D.W., Branson, C.C., Casey, R., Chavan, A., Coogan, A.H.,
644 Dechaseaux, C., Fleming, C.A., Haas, F., Hertlein, L.G., Kauffman, E.G., Keen A.M.,
645 Larocque, A., McAlester, A.L., Moore, R.C., Nuttall, C.P., Perkins, B.F., Purl, H.S.,
646 Smith, L.A., Soot-Ryen, T., Stenzel, H.B., Trueman, E.R., Turner, R.T., Weir J. (1971).
647 Part N. Mollusca (Bivalvia). In: Moore, R.C. (Ed.), Treatise of Invertebrate Paleontology.
648 Lawrence, Meriden and New York, The University of Kansas Printing Service, N1-
649 N1224.

650 Crippa, G., Ye, F., Malinverno, C., Rizzi, A. (2016). Which is the best method to prepare
651 invertebrate shells for SEM analysis? Testing different techniques on recent and fossil
652 brachiopods. Bollettino della Società Paleontologica Italiana, 55, 111-125.
653 D'Anastasi, B., Simpfendorfer, C., van Herwerden, L. (2013). *Anoxypristis cuspidata*. In: The
654 IUCN Red List of Threatened Species 2013: e.T39389A18620409.
655 http://www.iucnredlist.org, accessed on April 28, 2018.
656 DeVries, T.J. (2002). Patterns of diversity in Cenozoic marine mollusks from the Peruvian
657 province. Geological Society of America Abstracts with Programs, 34, 39.
658 DeVries, T.J. (2007). Molluscan evidence bearing on Cenozoic warm upwelling off southern
659 Peru. Geological Society of America Abstracts with Programs, 39, 78.
660 DeVries, T.J., Jud, N.A. (2018). Lithofacies patterns and paleogeography of the Miocene
661 Chilcatay and lower Pisco depositional sequences (East Pisco Basin, Peru). Boletín de la
662 Sociedad Geológica del Perú, Volumen Jubilar, 8, 124-167.
663 DeVries, T.J. (1998). Oligocene deposition and Cenozoic sequence boundaries in the Pisco
664 Basin (Peru). Journal of South American Earth Sciences, 11, 217-231.
665 DeVries, T.J. (2016). Fossil Cenozoic crassatelline bivalves from Peru: New species and
666 generic insights. Acta Palaeontologica Polonica, 61, 661-688.
667 DeVries, T.J., Frassinetti, D. (2003). Range extensions and biogeographic implications of
668 Chilean Neogene mollusks found in Peru. Boletín del Museo Nacional de Historia Natural,
669 Chile, 52, 119-135.
670 DeVries, T.J., Groves, L.T., Urbina, M. (2006). A new early miocene Muracypraea
671 Woodring, 1957 (Gastropoda: Cypraeidae) from the Pisco Basin of southern Peru. The
672 Nautilus, 120, 101-105.
673 DeVries, T.J., Schrader, H. (1997). Middle Miocene marine sediments in the Pisco Basin
674 (Peru). Boletín de la Sociedad Geológica del Perú, 87, 1-13.

675 Di Celma, C., Malinverno, E., Bosio, G., Collareta, A., Gariboldi, K., Gioncada, A., Molli,
676 G., Basso, D., Varas-Malca, R.M., Pierantoni, P.P., Villa, I.M., Lambert, O., Landini, W.,
677 Sarti, G., Cantalamessa, G., Urbina, M., Bianucci, G. (2017). Sequence stratigraphy and
678 paleontology of the upper Miocene Pisco Formation along the western side of the lower
679 Ica valley (Ica Desert, Peru). Rivista Italiana Paleontologia e Stratigrafia, 123, 255-274.
680 Di Celma, C., Malinverno, E., Bosio, G., Gariboldi, K., Collareta, A., Gioncada, A., Landini,
681 W., Pierantoni, P.P., Bianucci, G. (2018b). Intraformational unconformities as a record of
682 late Miocene eustatic falls of sea level in the Pisco Formation (southern Peru). Journal of
683 Maps, 14, 607-619.
684 Di Celma, C., Malinverno, E., Collareta, A., Bosio, G., Gariboldi, K., Lambert, O., Landini,
685 W., Gioncada, A., Villa, I.M., Coletti, G., de Muizon, C., Urbina, M., Bianucci, G.
686 (2018a). Facies analysis, stratigraphy and marine vertebrate assemblage of the early
687 Miocene Chilcatay Formation at Ullujaya (Pisco basin, Peru). Journal of Maps, 14, 257-
688 268.
689 Di Celma, C., Pierantoni, P.P., Malinverno, E., Collareta, A., Lambert, O., Landini, W.,
690 Bosio, G., Gariboldi, K., Gioncada, A., de Muizon, C., Molli, G., Marx, F.G., Varas-
691 Malca, R.M., Urbina, M., Bianucci, G. (2019). Allostratigraphy and paleontology of the
692 lower Miocene Chilcatay Formation in the Zamaca area, East Pisco basin, southern Peru.
693 Journal of Maps, 15, 393-405.
694 Dunbar, R.B., Marty, R.C., Baker, P.A. (1990). Cenozoic marine sedimentation in the
695 Sechura and Pisco basins, Peru. Palaeogeography, Palaeoclimatology, Palaeoecology, 77,
696 235-261.
697 Ebersole, J.A., Ebersole, S.M., Cicimurri, D.J. (2017). The occurrence of early Pleistocene
698 marine fish remains from the Gulf Coast of Mobile County, Alabama, USA.
699 Palaeodiversity, 10, 97-116.

Enax, J., Janus, A. M., Raabe, D., Epple, M., Fabritius, H. O. (2014). Ultrastructural organization and micromechanical properties of shark tooth enameloid. Acta Biomaterialia, 10, 3959-3968.

Faure, G., Mensing, T.M. (2005). Isotopes: Principles and Applications. New York, John Wiley & Sons.

Föllmi, K.B. (2016). Sedimentary condensation. Earth-Science Reviews, 152, 143-180.

Frijia, G., Parente, M. (2008). Strontium isotope stratigraphy in the upper Cenomanian shallow-water carbonates of the southern Apennines: Short-term perturbations of marine $^{87}Sr/^{86}Sr$ during the oceanic anoxic event 2. Palaeogeography, Palaeoclimatology, Palaeoecology, 261, 15-29.

Frijia, G., Parente, M., Di Lucia, M., Mutti, M. (2015). Carbon and strontium isotope stratigraphy of the Upper Cretaceous (Cenomanian-Campanian) shallow-water carbonates of southern Italy: Chronostratigraphic calibration of larger foraminifera biostratigraphy. Cretaceous Research, 53, 110-139.

Gariboldi, K., Bosio, G., Malinverno, E., Gioncada, A., Di Celma, C., Villa, I.M., Urbina, M., Bianucci, G. (2017). Biostratigraphy, geochronology and sedimentation rates of the upper Miocene Pisco Formation at two important marine vertebrate fossil-bearing sites of southern Peru. Newsletters on Stratigraphy, 50, 417-444.

Gariboldi, K., Gioncada, A., Bosio, G., Malinverno, E., Di Celma, C., Tinelli, C., Cantalamessa, G., Landini, W., Urbina, M., Bianucci, G. (2015). The dolomite nodules enclosing fossil marine vertebrates in the East Pisco Basin, Peru: field and petrographic insights into the Lagerstätte formation. Palaeogeography, Palaeoclimatology, Palaeoecology, 438, 81-95.

723 Gioncada, A., Collareta, A., Gariboldi, K., Lambert, O., Di Celma, C., Bonaccorsi, E.,
724 Urbina, M., Bianucci, G. (2016). Inside baleen: exceptional microstructure preservation in
725 a late Miocene whale skeleton from Peru. Geology, 44, 839-842.
726 Gioncada, A., Gariboldi, K., Collareta, A., Di Celma, C., Bosio, G., Malinverno, E., Lambert,
727 O., Pike, J., Urbina, M., Bianucci, G. (2018a). Looking for the key to preservation of fossil
728 marine vertebrates in the Pisco Formation of Peru: new insights from a small dolphin
729 skeleton. Andean Geology, 45, 379-398.
730 Gioncada, A., Petrini, R., Bosio, G., Gariboldi, K., Collareta, A., Malinverno, E., Bonaccorsi,
731 E., Di Celma, C., Pasero, M., Urbina, M., Bianucci, G. (2018b). Insights into the
732 diagenetic environment of fossil marine vertebrates of the Pisco Formation (late Miocene,
733 Peru) from mineralogical and Sr-isotope data. Journal of South American Earth Sciences,
734 81, 141-152.
735 Hampel, A., Kukowski, N., Bialas, J., Heubscher, C., Heinbockel, R. (2004). Ridge
736 subduction at an erosive margin: the collision zone of the Nazca Ridge in southern Peru.
737 Journal of Geophysical Research, 109, article #B02101.
738 Hsu, J.T., 1992. Quaternary uplift of the Peruvian coast related to the subduction of the Nazca
739 Ridge: 13.5 to 15.6 degrees South latitude. Quaternary International, 15/16, 87-97.
740 Kellogg, R. (1965). Fossil marine mammals from the Miocene Calvert Formation of
741 Maryland and Virginia, part 1: a new whalebone whale from the Miocene Calvert
742 Formation. United States National Museum Bulletin, 247, 1-45.
743 Kimura, T., Hasegawa, Y., Ohzawa, H., Yamaoka, T., Furukawa, Y., Ueda, T., Kiyoshi, T.,
744 Sugihara, M., Sakuda, M. (2007). A mysticete whale (Cetacea) skeleton from the middle
745 Miocene Bihoku Group, Shobara, Hiroshima, Japan. Miscellaneous Reports of the Hiwa
746 Museum for Natural History, 48, 1-10.

747 Kulm, L.D., Resig, J.M., Thornburg, T.M., Schrader, H.J. (1982). Cenozoic structure,
748 stratigraphy and tectonics of the central Peru forearc. In: Legget, J.K. (Ed.), Trench and
749 forearc geology: sedimentation and tectonics on modern and ancient plate margins.
750 London, Blackwells, 151-169.
751 Lambert, O., Bianucci, G., de Muizon, C. (2017a). Macroraptorial sperm whales (Cetacea,
752 Odontoceti, Physeteroidea) from the Miocene of Peru. Zoological Journal of the Linnean
753 Society, 179, 404-474.
754 Lambert, O., Bianucci, G., Urbina, M. (2014). *Huaridelphis raimondii*, a new early Miocene
755 Squalodelphinidae (Cetacea, odontoceti) from the Chilcatay Formation, Peru. Journal of
756 Vertebrate Paleontology, 34, 987-1004.
757 Lambert, O., Bianucci, G., Urbina, M., Geisler, J.H. (2017b). A new inioid (Cetacea,
758 Odontoceti, Delphinidae) from the Miocene of Peru and the origin of modern dolphin and
759 porpoise families. Zoological Journal of the Linnean Society, 179, 919-946.
760 Lambert, O., de Muizon, C., Malinverno, E., Di Celma, C., Urbina, M., Bianucci, G. (2018).
761 A new odontocete (toothed cetacean) from the Early Miocene of Peru expands the
762 morphological disparity of extinct heterodont dolphins. Journal of Systematic
763 Palaeontology, 16, 981-1016.
764 Lambert, O., de Muizon, C., Bianucci, G. (2015). A new archaic homodont toothed cetacean
765 (Mammalia, Cetacea, Odontoceti) from the early Miocene of Peru. Geodiversitas, 37, 79-
766 108.
767 Landini, W., Altamirano-Sierra, A., Collareta, A., Di Celma, C., Urbina, M., Bianucci, G.
768 (2017a). The late Miocene elasmobranch assemblage from Cerro Colorado (Pisco
769 Formation, Peru). Journal of South American Earth Sciences, 73, 168-190.

770 Landini, W., Collareta, A., Pesci, F., Di Celma, C., Urbina, M., Bianucci, G. (2017b). A
771 secondary nursery area for the copper shark *Carcharhinus brachyurus* from the late
772 Miocene of Peru. Journal of South American Earth Sciences, 78, 164-174.
773 Landini, W., Collareta, A., Di Celma, C., Malinverno, E., Urbina, M., Bianucci, G. (2019)
774 The early Miocene elasmobranch assemblage from Zamaca (Chilcatay Formation, Peru).
775 Journal of South American Earth Sciences, 91, 352-371.
776 León, W., Aleman, A., Torres, V., Rosell, W., De la Cruz, O. (2008). Estratigrafía,
777 sedimentología y evolución tectónica de la cuenca Pisco Oriental. Boletín INGEMMET,
778 27, 144 pp.
779 Macharé J., Ortlieb L. (1992). Plio-Quaternary vertical motions and the subduction of the
780 Nazca Ridge, central coast of Peru. Tectonophysics, 205, 97-108.
781 Marocco R., de Muizon C., (1988). Le Bassin Pisco, bassin cénozoïque d'avant arc de la côte
782 du Pérou central: analyse géodynamique de son remplissage. Géodynamique, 3, 3-19.
783 Marx F.G., Collareta A., Gioncada A., Post K., Lambert O., Bonaccorsi E., Urbina M.,
784 Bianucci G. (2017a). How whales used to filter: exceptionally preserved baleen in a
785 Miocene cetotheriid. Journal of Anatomy, 231, 212-220.
786 Marx, F.G., Fitzgerald, E.M., Fordyce, R. E. (2019). Like phoenix from the ashes: How
787 modern baleen whales arose from a fossil "dark age". Acta Palaeontologica Polonica, 64,
788 231-238.
789 Marx, F.G., Lambert, O., de Muizon, C. (2017b). A new Miocene baleen whale from Peru
790 deciphers the dawn of cetotheriids. Royal Society Open Science, 4, article #170560.
791 McArthur, J. (1994). Recent Trends in Strontium Isotope Stratigraphy. Terra Nova, 6, 331-
792 358.

McArthur, J.M., Howarth, R.J., Shields, G.A. (2012). Strontium Isotope Stratigraphy. In: Gradstein, F.M., Ogg, J.G., Schmitz, M., Ogg, G. (Eds.), The Geologic Time Scale 2012. Oxford, Elsevier, 127-144.

Nielsen, S.N., Glodny, J. (2009). Early Miocene subtropical water temperatures in the southeast Pacific. Palaeogeography, Palaeoclimatology, Palaeoecology, 280, 480-488.

North American Commission on Stratigraphic Nomenclature [NACSN] (2005). North American stratigraphic code. American Association of Petroleum Geologists Bulletin, 89, 1547-1591.

Perez, V.J., Godfrey, S.J., Kent, B.W., Weems, R.E., Nance, J.R. (2018). The transition between Carcharocles chubutensis and Carcharocles megalodon (Otodontidae, Chondrichthyes): lateral cusplet loss through time. Journal of Vertebrate Paleontology, 38, article #e1546732.

Pilger R.H. (1981). Plate reconstructions, aseismic ridges, and low-angle subduction beneath the Andes. Geological Society of America Bulletin, 92, 448-456.

Santos, A., Mayoral, E., Muñiz, F. (2005). Bioerosion scars of acorn barnacles from the southwestern Iberian Peninsula, upper Neogene. Rivista Itliana di Paleontologia e Stratigrafia, 111, 181-189.

Scasso, R.A., McArthur, J.M., del Río, C.J., Martínez, S., Thirlwall, M.F. (2001). $^{87}Sr/^{8}6Sr$ Late Miocene age of fossil molluscs in the “Entrerriense” of the Valdés Peninsula (Chubut, Argentina). Journal of South American Earth Sciences, 14, 319-329.

Steuber, T. (1999). Isotopic and chemical intra-shell variations in low-Mg calcite of rudist bivalves (Mollusca: Hippuritacea): disequilibrium fractionations and Late Cretaceous seasonality. International Journal Earth Sciences, 88, 551-570.

Steuber, T. (2003). Strontium isotope chemostratigraphy of rudist bivalves and cretaceous carbonate platforms. In: Gili, E., Negra, M.E.H., Skelton, P.W. (Eds.), North African

Cretaceous Carbonate Platform Systems. NATO Science Series, IV. Earth and Environmental Sciences, 28, 229-238.

Thornburg, T.M., Kulm, L.D. (1981). Sedimentary basins of the Peru continental margin: structure, stratigraphy, and Cenozoic tectonics from 6ºS to 16ºS latitude. In: Kulm, L.D., Dymond, J., Dasch, E.J., Hussong, D.M. (Eds.), Nazca plate: crustal formation and Andean convergence. Geological Society of America Memoir, 154, 393-422.

Travis, R. B., Gonzales, G., Pardo, A. (1974). Hydrocarbon Potential of Coastal Basins of Peru. AAPG Bulletin, 58, 1460-1460.

Ullmann, C.V., Korte, C. (2015). Diagenetic alteration in low-Mg calcite from macrofossils: a review. Geological Quarterly, 59, 3-20.

Zúñiga-Rivero, F.J., Klein, G.D., Hay-Roe, H., Álvarez-Calderon, E. (2010). The hydrocarbon potential of Peru. Lima, BPZ Exploración & Producción S.R.L.

Figure captions

Figure 1. A. Map of the major Cenozoic sedimentary basins along the Peruvian coast. Major structural highs are the Coastal Batholith, the Outer Shelf High and the Upper Slope Ridge. The red dashed rectangle outlines location of the area shown in detail in panel B. Redrawn and modified from Travis et al. (1976) and Thornburg and Kulm (1981). **B.** Paleoenvironmental reconstruction of the Peruvian coast during the Miocene. Islands are hypothesized on the basis of the distribution of the pre-Cenozoic rocks. Redrawn and modified from DeVries and Schrader (1997).

Figure 2. A. Satellite image of the localities of Cerro Submarino, Ullujaya, and Roca Negra along the western side of the Ica River (Ica desert). Based on a Google Earth image (© 2018 DigitalGlobe). **B.** Schematic stratigraphic sections measured at the Chilcatay outcrops of Ullujaya (UL) and Roca Negra (RN) that show the stratigraphic position of the investigated beds and the ^{39}Ar–^{40}Ar ages obtained from tephra layers. **C.** Field photo at Cerro Submarino, with the location of the samples (blue stars) collected from the P0 sequence. The PE0.0 and PE0.1 unconformities are traced in red.

Figure 3. A. Oyster shell from the PN Oyster level in the Ct1 sequence at Roca Negra. Note the predation holes on the outer part of the shell. **B.** Pectinid specimen from the mollusk- and barnacle-rich horizon in the Ct1 sequence at Ullujaya. Note the small drill holes and the barnacle attachment scars (i.e., *Anellusichnus*). **C.** Barnacle plate from the Key bed C in the Ct1 sequence at Ullujaya. Note the lamellar sheath (i.e., the thickened upper part of the inner wall) from which the SIS samples were taken. **D.** Tooth of *Cosmopolitodus hastalis* from the P0 sequence at Cerro Submarino.

Figure 4. A, B. Transmitted light and cathodoluminescence microscopical photo of a pectinid shell. **C, D.** Transmitted light and cathodoluminescence microscopical photo of an oyster prismatic layer with a low and homogeneous luminescence, punctuated by microborings with a high luminescence. **E, F.** Transmitted light and catodoluminescence microscopical photo of a poorly preserved oyster shell, characterized by an alternation of high luminescent layers of sparry calcite. **G, H.** Transmitted light and catodoluminescence microscopical photo of the transverse thin section of a barnacle shell showing tree-like interlaminate figures and the parietal tubes filled by diagenetic calcite with a high luminescence.

Figure 5. A. SE (Secondary Electron) image of an oyster cross-section. Note the alternation of different layers. **B.** Close-up of the oyster shell depicted in panel A. Note the alternation of prismatic layers (light grey) and sparry calcite layers (dark grey). **C.** SE image of a well-preserved prismatic layer of an oyster. **D.** SE image of a poorly preserved oyster shell exhibiting dissolution features.

Figure 6. Diagenetic path diagrams, showing the major trends of diagenetic alteration. **A.** Multi-component plot of $^{87}Sr/^{86}Sr$ ratio vs Sr concentration. **B.** Multi-component plot of $^{87}Sr/^{86}Sr$ ratio vs Fe concentration. **C.** Multi-component plot of $^{87}Sr/^{86}Sr$ ratio vs Mn concentration. **D.** Multi-component plot of Sr vs Mn concentrations. Arrows indicate trends of diagenetic alteration.

Figure 7. Fossils of warm-water taxa from the P0 sequence. **A, B, C.** Cypraeid specimen in lateral (A), dorsal (B), and apertural (C) views. **D, E.** Tooth of *Hemipristis serra* in lingual (A) and labial (B) views. **F.** Rhizangiid corallites encrusting a cluster of barnacle shells. **G.**

880 Close-up of the corallites depicted in panel F. **H, I, J.** Architectonicid specimen in lateral (H),
881 dorsal (I), and ventral (J) views.
882
883 **Figure 8.** Schematic chronostratigraphic section of the Chilcatay (Ct1 and Ct2) and Pisco (P0
884 and P1) sequences according to Strontium Isotope Stratigraphy.

885 **Table captions**

886

887 **Table 1.** Sample list and description, with locality and stratigraphic data.

888

889 **Table 2.** Strontium isotope analysis results, reporting $^{87}Sr/^{86}Sr$ values and standard

890 deviations, with corrections based on the NIST NBS 987 and USGS EN-1 standards.

891

892 **Table 3.** $^{87}Sr/^{86}Sr$ ages for the Ct1 and P0 sequences, calculated from the LOWESS Table 5

893 (McArthur et al., 2012).

Figure 1

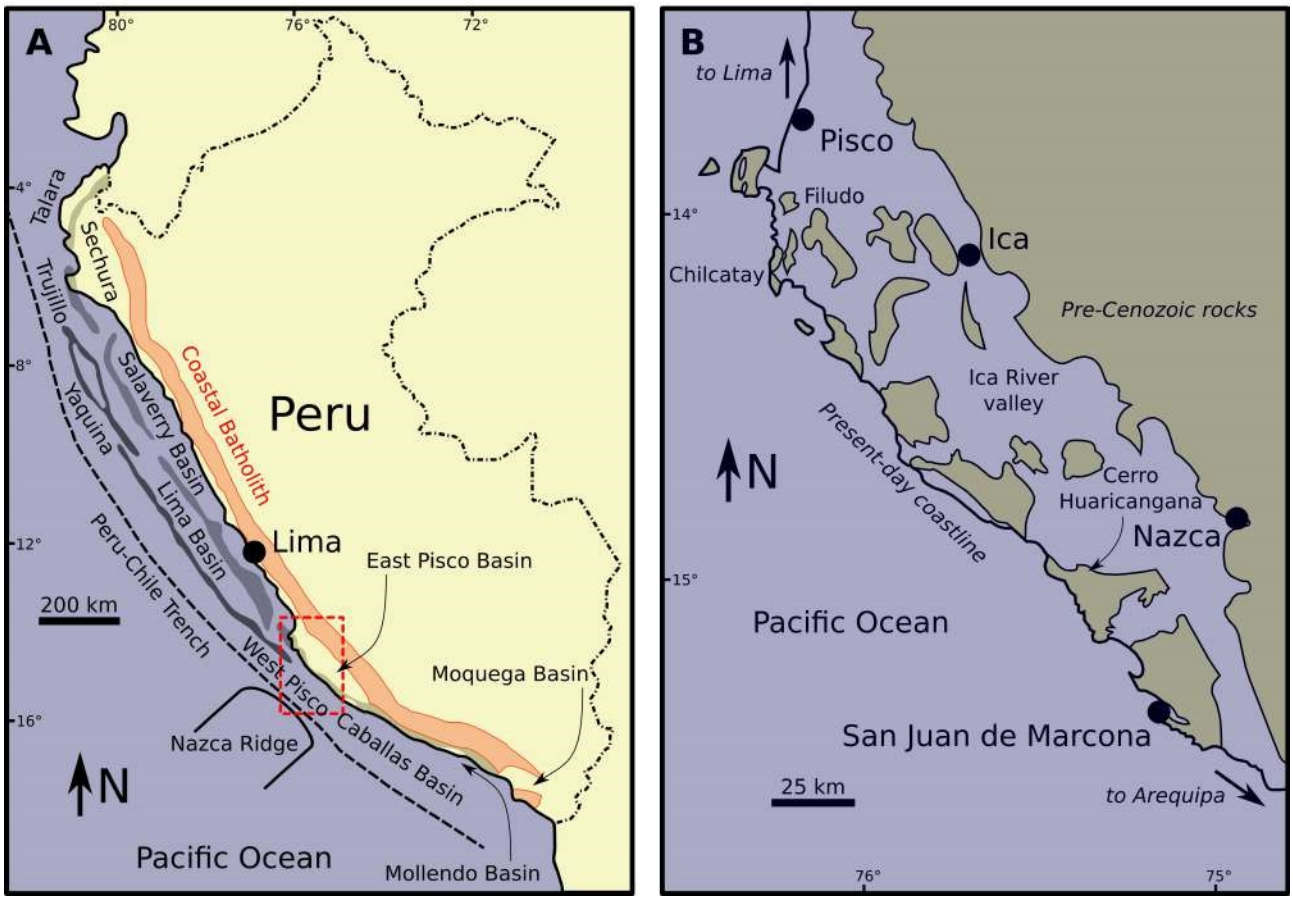
A
80°
76°
72°
4°
8°
12°
16°
Talara
Sechura
Trujillo
Salaverry Basin
Yaquina
Lima Basin
Peru-Chile Trench
Coastal Batholith
Peru
Lima
East Pisco Basin
Moquega Basin
West Pisco
Caballas Basin
Nazca Ridge
200 km
N
Pacific Ocean
Mollendo Basin
B
to Lima
Pisco
Filudo
14°
Chilcatay
Ica
Pre-Cenozoic rocks
Ica River
valley
Present-day coastline
N
Cerro
Huaricangana
Nazca
15°
Pacific Ocean
San Juan de Marcona
25 km
to Arequipa
76°
75°

Figure 2

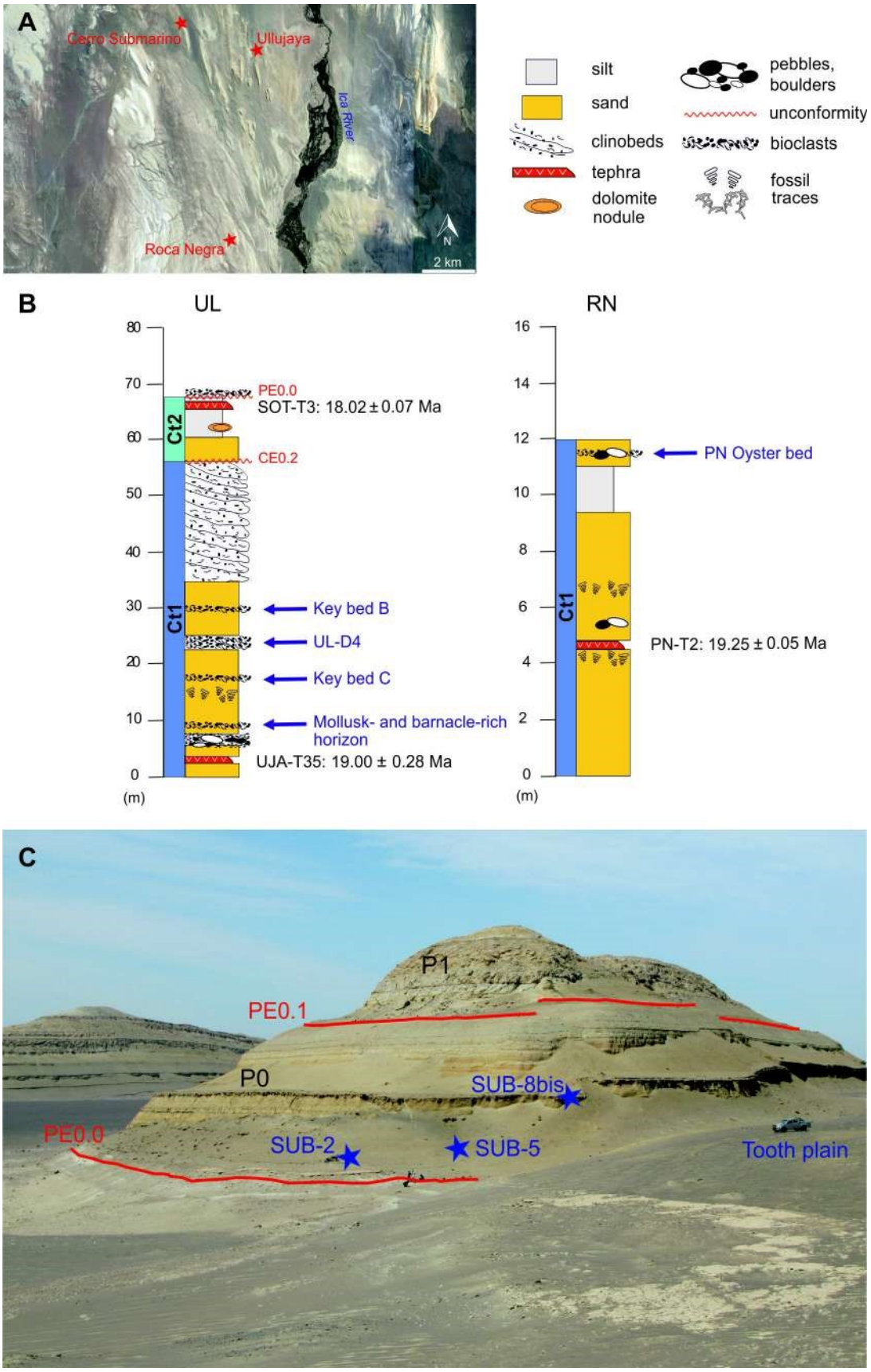
A
Cerro Submarino
Ullujaya
Ica River
Roca Negra
N
2 km
silt
sand
clinobeds
tephra
dolomite nodule
pebbles, boulders
unconformity
bioclasts
fossil traces
B
UL
RN
(m)
Ct2
Ct1
PE0.0
SOT-T3: 18.02 ± 0.07 Ma
CE0.2
Key bed B
UL-D4
Key bed C
Mollusk- and barnacle-rich horizon
UJA-T35: 19.00 ± 0.28 Ma
PN Oyster bed
PN-T2: 19.25 ± 0.05 Ma
C
P1
PE0.1
P0
SUB-8bis
PE0.0
SUB-2
SUB-5
Tooth plain

Figure 3

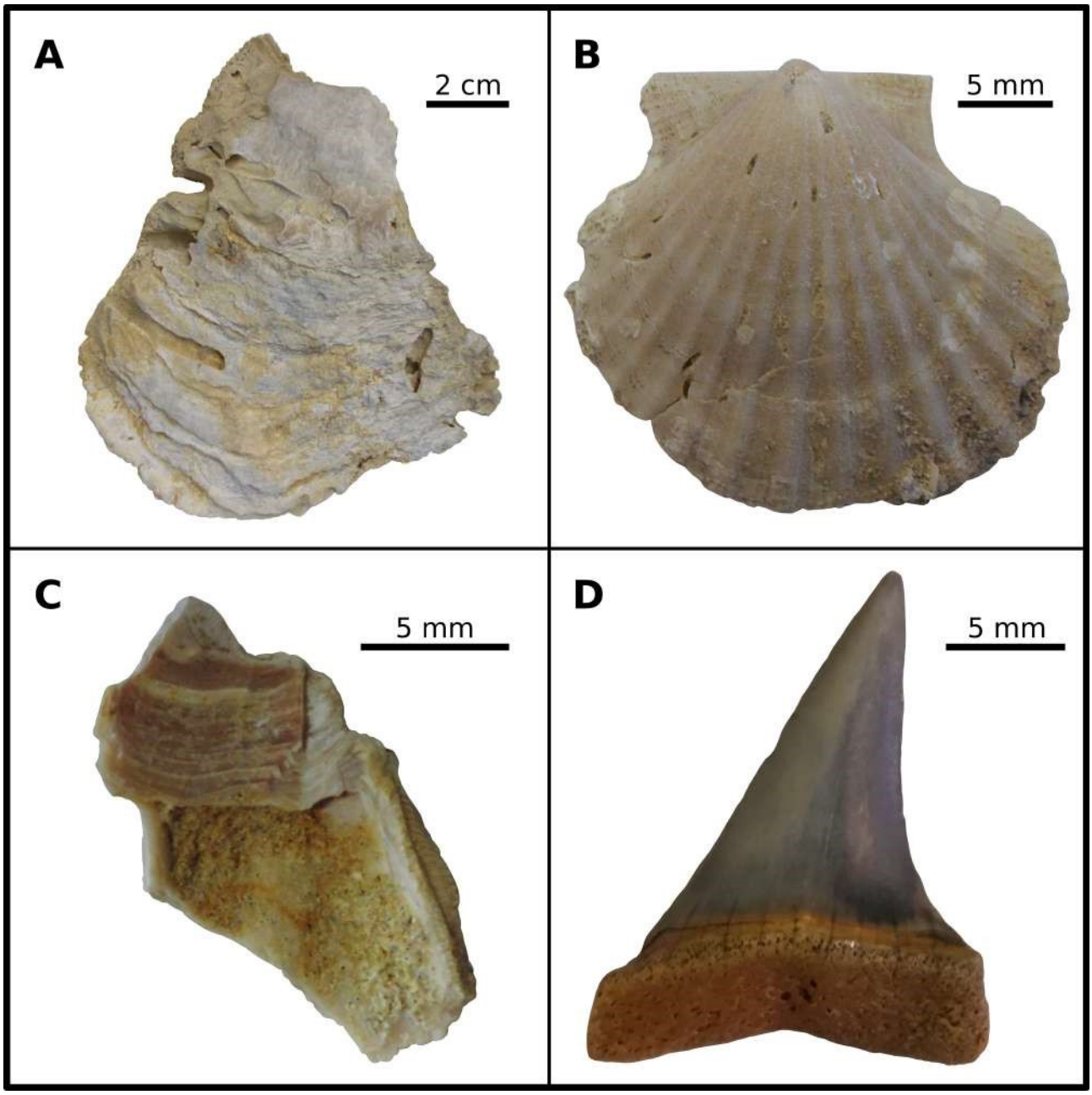

Figure 4

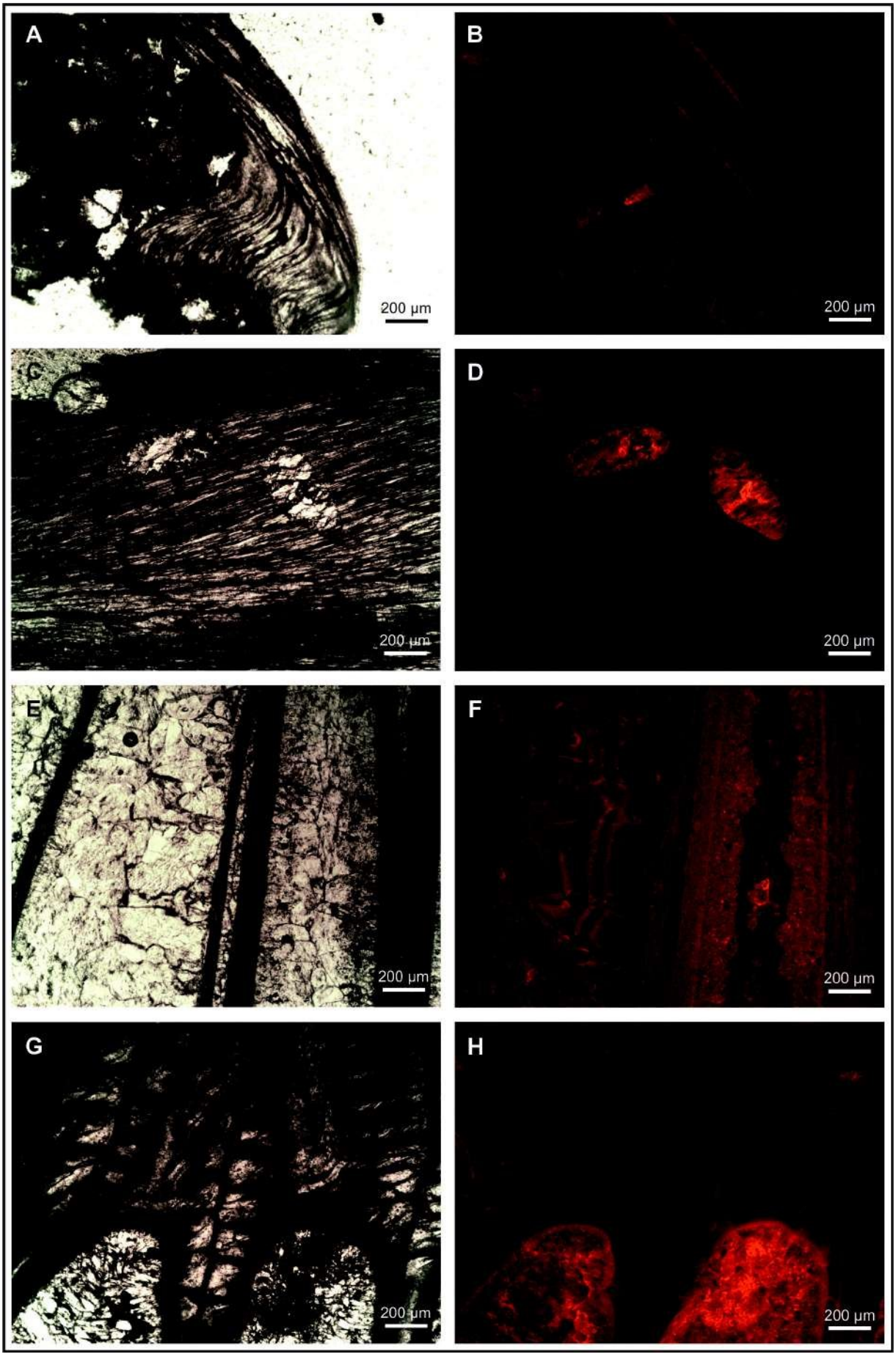

Figure 5

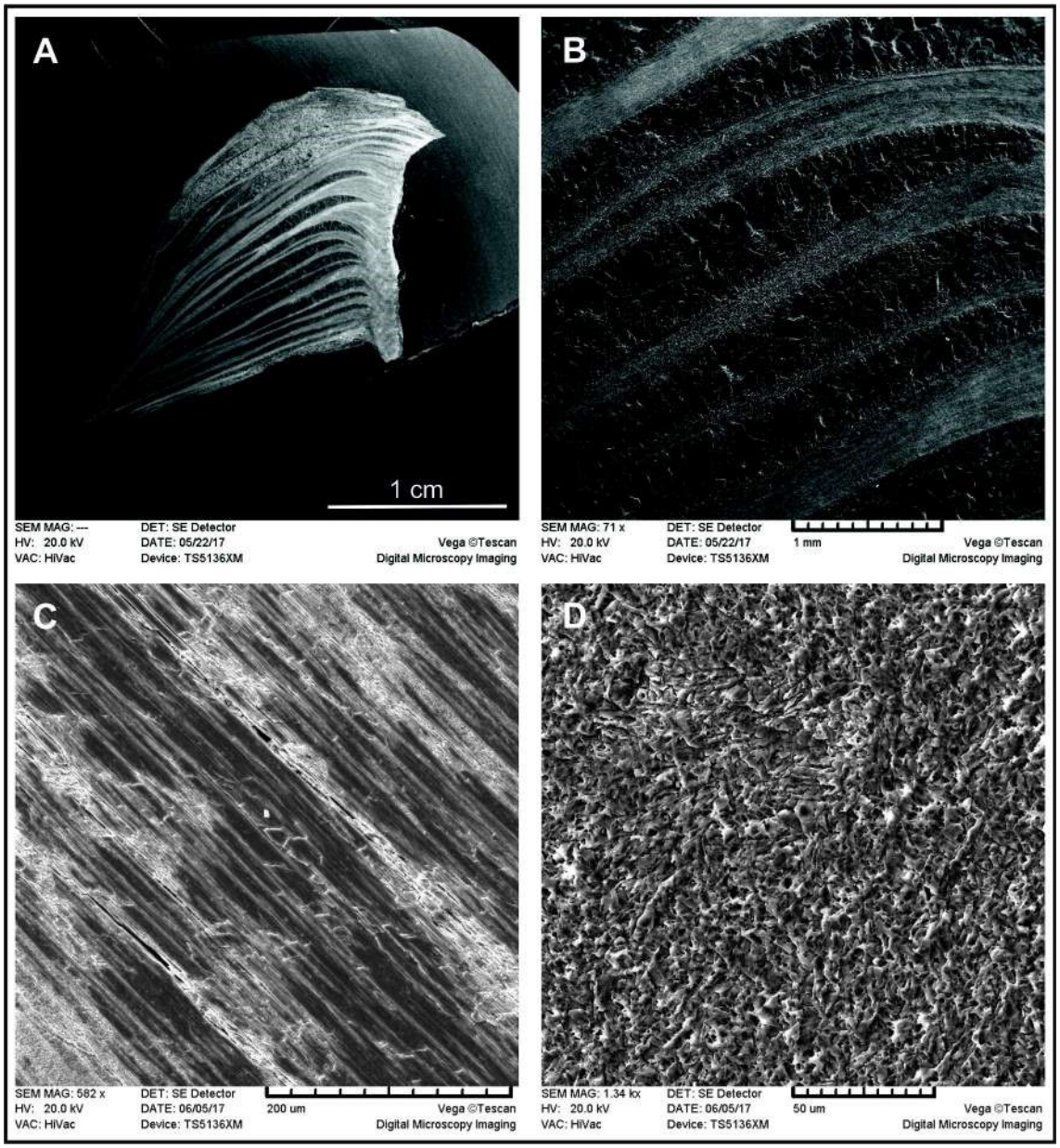
A
1 cm
SEM MAG: ---
HV: 20.0 kV
VAC: HiVac
DET: SE Detector
DATE: 05/22/17
Device: TS5136XM
Vega ©Tescan
Digital Microscopy Imaging
B
SEM MAG: 71 x
HV: 20.0 kV
VAC: HiVac
DET: SE Detector
DATE: 05/22/17
Device: TS5136XM
1 mm
Vega ©Tescan
Digital Microscopy Imaging
C
SEM MAG: 582 x
HV: 20.0 kV
VAC: HiVac
DET: SE Detector
DATE: 06/05/17
Device: TS5136XM
200 um
Vega ©Tescan
Digital Microscopy Imaging
D
SEM MAG: 1.34 kx
HV: 20.0 kV
VAC: HiVac
DET: SE Detector
DATE: 06/05/17
Device: TS5136XM
50 um
Vega ©Tescan
Digital Microscopy Imaging

Figure 6

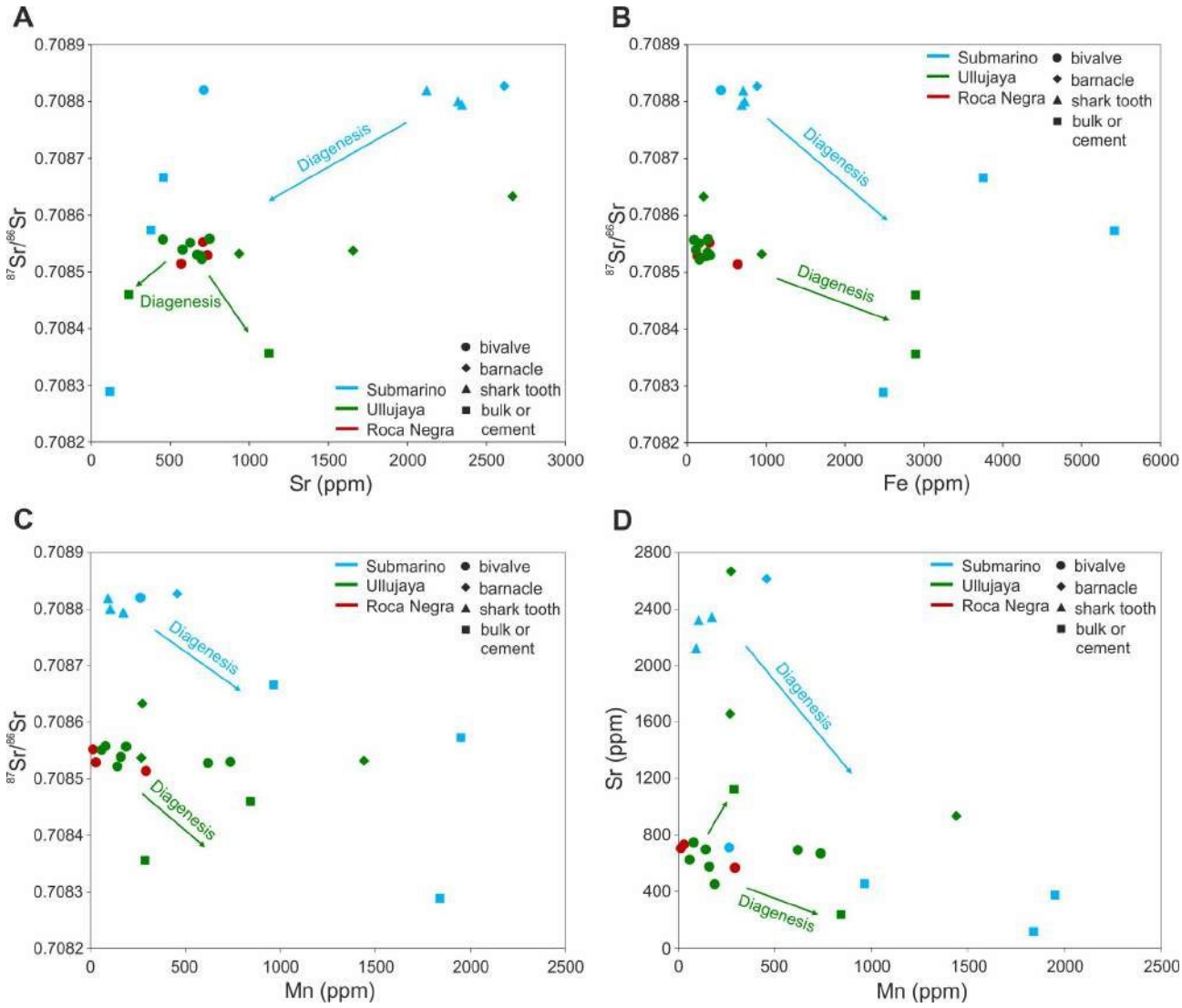
A
B
C
D
Diagenesis
Submarino
Ullujaya
Roca Negra
bivalve
barnacle
shark tooth
bulk or cement
$^{87}Sr/^{86}Sr$
Sr (ppm)
Fe (ppm)
Mn (ppm)

Figure 7

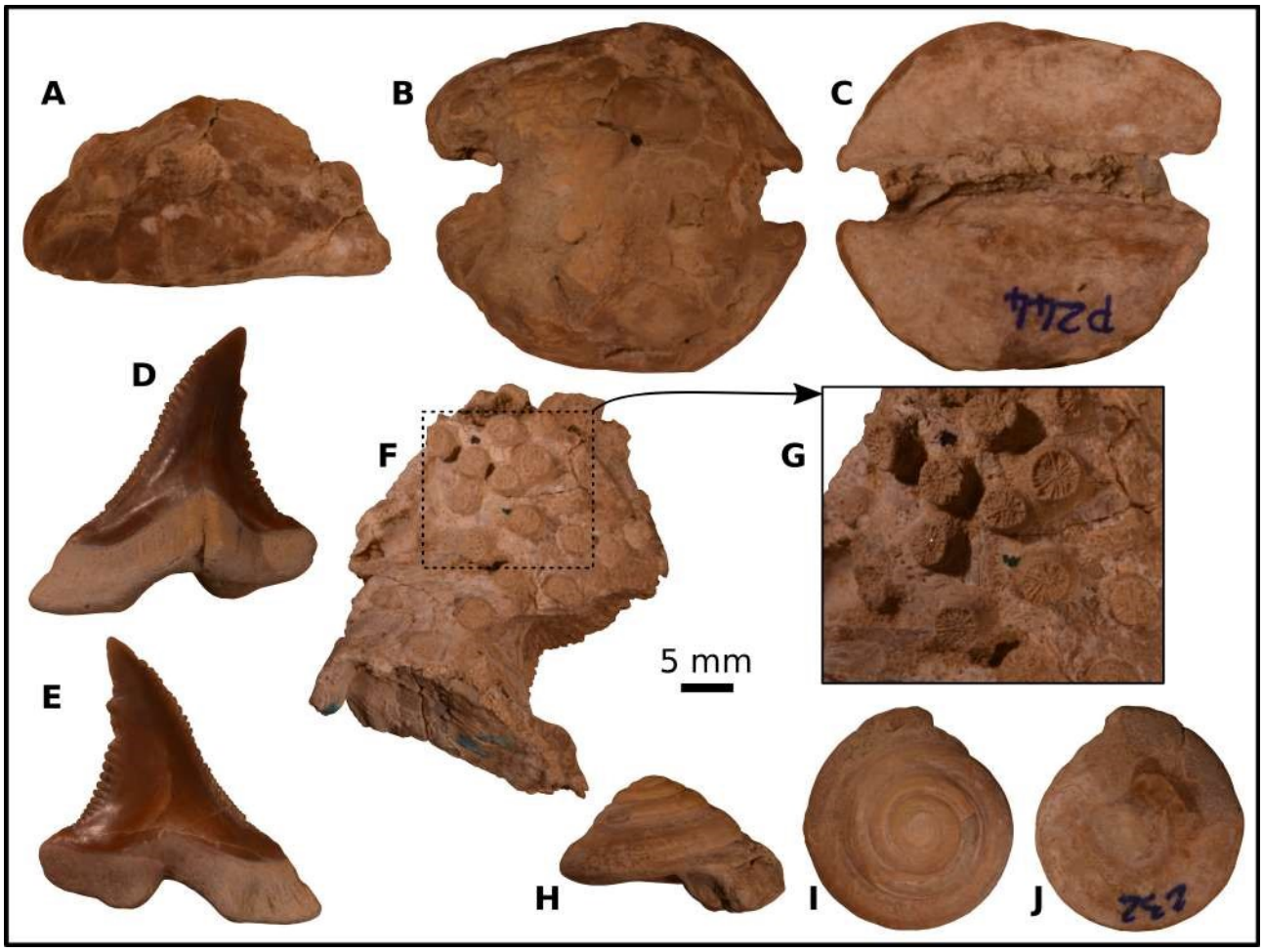

Figure 8

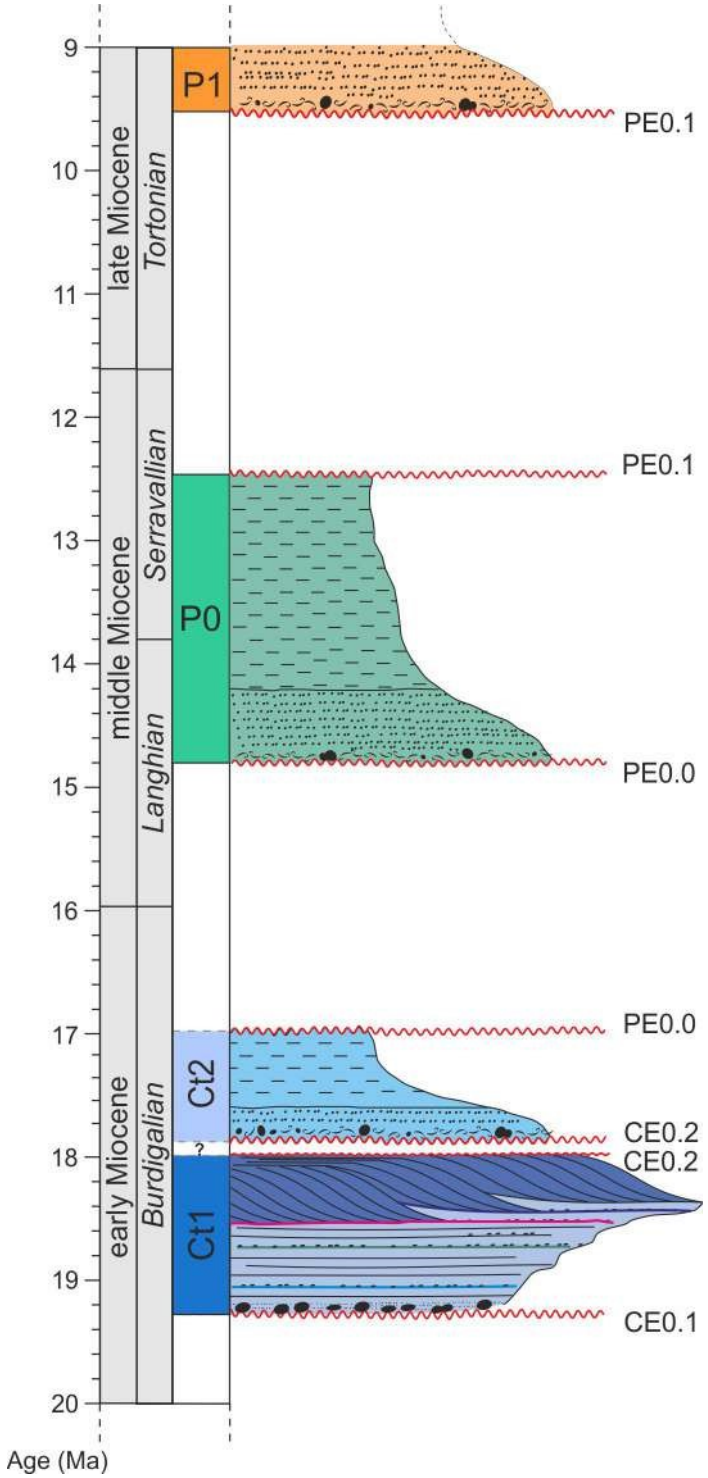
9
10
11
12
13
14
15
16
17
18
19
20
Age (Ma)
late Miocene
middle Miocene
early Miocene
Tortonian
Serravallian
Langhian
Burdigalian
P1
P0
Ct2
Ct1
PE0.1
PE0.1
PE0.0
PE0.0
CE0.2
CE0.2
CE0.1

Table 1

Sample	Locality	Formation	Sequence	Stratigraphic level	Description
SUB-8bis1	Cerro Submarino	Pisco	P0	Undifferentiated P0 (SUB-8bis)	Barnacle sheath
SUB-8bis2	Cerro Submarino	Pisco	P0	Undifferentiated P0 (SUB-8bis)	Bulk sediment cemented inside a barnacle test
SUB-8bis3	Cerro Submarino	Pisco	P0	Undifferentiated P0 (SUB-8bis)	Recrystallized bivalve shell
SUB-5	Cerro Submarino	Pisco	P0	Undifferentiated P0 (SUB-5)	Ostreid specimen
SUB-2	Cerro Submarino	Pisco	P0	Undifferentiated P0 (SUB-2)	Calcite nodule
Tooth 1	Cerro Submarino	Pisco	P0	Undifferentiated P0 (tooth plain)	Shark tooth: *Cosmopolitodus hastalis*
Tooth 2	Cerro Submarino	Pisco	P0	Undifferentiated P0 (tooth plain)	Shark tooth: *Cosmopolitodus hastalis*
Tooth 3	Cerro Submarino	Pisco	P0	Undifferentiated P0 (tooth plain)	Shark tooth: *Isurus oxyrinchus*
UJA-2a	Ullujaya	Chilcatay	Ct1	Key bed B	Ostreid specimen
UJA-2b	Ullujaya	Chilcatay	Ct1	Key bed B	Ostreid specimen
UL-D4a	Ullujaya	Chilcatay	Ct1	UL-D4	Ostreid specimen
UL-D4b	Ullujaya	Chilcatay	Ct1	UL-D4	Barnacle sheath
UL-D4c	Ullujaya	Chilcatay	Ct1	UL-D4	Bulk sediment cemented inside a barnacle test
UJA-LIVC1	Ullujaya	Chilcatay	Ct1	Key bed C	Ostreid specimen
UJA-LIVC2	Ullujaya	Chilcatay	Ct1	Key bed C	Bulk sediment cemented outside an oyster
UJA-LIVC3	Ullujaya	Chilcatay	Ct1	Key bed C	Ostreid specimen
UJA-LIVC4	Ullujaya	Chilcatay	Ct1	Key bed C	Barnacle sheath
UL-LIVa	Ullujaya	Chilcatay	Ct1	Mollusk- and barnacle-rich horizon	Barnacle sheath
UL-LIVb	Ullujaya	Chilcatay	Ct1	Mollusk- and barnacle-rich horizon	Pectinid specimens
UL-LIVd	Ullujaya	Chilcatay	Ct1	Mollusk- and barnacle-rich horizon	Pectinid specimen
PN-OST	Roca Negra	Chilcatay	Ct1	PN Oyster bed	Ostreid specimen
PN-GIO1	Roca Negra	Chilcatay	Ct1	PN Oyster bed	Ostreid specimen
PN-GIO2	Roca Negra	Chilcatay	Ct1	PN Oyster bed	Ostreid specimen

Table 2

Sample	measured $^{87}Sr/^{86}Sr$	± 2 σ_{mean}	$^{87}Sr/^{86}Sr$ sample corrected to difference between the NIST NBS 987 value of McArthur and the NIST NBS 987 value	$^{87}Sr/^{86}Sr$ sample corrected to difference between the USGS EN-1 value of McArthur and the USGS EN-1 value measured	$^{87}Sr/^{86}Sr$ sample corrected to difference between the NIST NBS 987 value of McArthur and the NIST NBS 987 mean value	$^{87}Sr/^{86}Sr$ sample corrected to difference between the USGS EN-1 value of McArthur and the USGS EN-1 mean value of
NIST NBS 987	*0.710252*	*0.000006*	*0.710247*	*0.710254*	*0.710258*	*0.710268*
PN-OST	0.708498	0.000005	0.708493	0.708500	0.708504	0.708514
PN-GI01	0.708513	0.000007	0.708508	0.708515	0.708519	0.708529
PN-GI02	0.708536	0.000005	0.708531	0.708538	0.708542	0.708552
UJA-2a	0.708541	0.000005	0.708536	0.708543	0.708547	0.708557
UJA-2b	0.708523	0.000005	0.708518	0.708525	0.708529	0.708539
UL-D4a	0.708506	0.000004	0.708501	0.708508	0.708512	0.708522
UL-D4b	0.708617	0.000005	0.708612	0.708619	0.708623	0.708633
UL-D4c	0.708444	0.000005	0.708439	0.708446	0.708450	0.708460
UL-LIVa	0.708516	0.000005	0.708511	0.708518	0.708522	0.708532
UL-LIVb	0.708512	0.000005	0.708507	0.708514	0.708518	0.708528
USGS EN-1	*0.709173*	*0.000005*	*0.709168*	*0.709175*	*0.709179*	*0.709189*
NIST NBS 987	*0.710235*	*0.000005*	*0.710247*	*0.710250*	*0.710241*	*0.710251*
UL-LIVd	0.708514	0.000005	0.708526	0.708529	0.708520	0.708530
UJA-LIVC1	0.708535	0.000005	0.708547	0.708550	0.708541	0.708551
UJA-LIVC2	0.708340	0.000005	0.708352	0.708355	0.708346	0.708356
UJA-LIVC3	0.708542	0.000005	0.708554	0.708557	0.708548	0.708558
UJA-LIVC4	0.708521	0.000005	0.708533	0.708536	0.708527	0.708537
SUB-5	0.708804	0.000005	0.708816	0.708819	0.708810	0.708820
SUB-2	0.708557	0.000005	0.708569	0.708572	0.708563	0.708573
USGS EN-1	*0.709160*	*0.000005*	*0.709172*	*0.709175*	*0.709166*	*0.709176*
NIST NBS 987	*0.710244*	*0.000005*	*0.710247*	*0.710252*	*0.710250*	*0.710260*
SUB-8bis1	0.708811	0.000005	0.708814	0.708819	0.708817	0.708827
SUB-8bis2	0.708273	0.000005	0.708276	0.708281	0.708279	0.708289
SUB-8bis3	0.708650	0.000005	0.708653	0.708658	0.708656	0.708666
Tooth1	0.708803	0.000005	0.708806	0.708811	0.708809	0.708819
Tooth2	0.708778	0.000005	0.708781	0.708786	0.708784	0.708794
Tooth3	0.708784	0.000005	0.708787	0.708792	0.708790	0.708800
USGS EN-1	*0.709167*	*0.000005*	*0.709170*	*0.709175*	*0.709173*	*0.709183*

Table 3

	Stratigraphic level	*minus 2 s.e.*	$^{87}Sr/^{86}Sr$ mean value	*plus 2 s.e.*	Maximum age (Ma)	Preferred age (Ma)	Minimum age (Ma)
P0	Lower P0	0.708799	0.708812	0.708825	14.80	13.45	12.45
Ct1	Key bed B	0.708530	0.708548	0.708566	18.60	18.30	18.00
	Key bed C	0.708536	0.708549	0.708561	18.50	18.30	18.10
	Mollusk- and barnacle-rich horizon	0.708528	0.708530	0.708532	18.60	18.50	18.40
	PN Oyster bed	0.708510	0.708532	0.708554	18.85	18.50	18.15